Probing Charm Production with Three-Particle Correlations in pp Collisions

Author
Kim Haupt

Supervisor
Alice Ohlson

Fysk03 for 15hp
May 2023
A Bachelor of Science Thesis

Department of Physics
Division of Particle and Nuclear Physics

LUND
UNIVERSITY

Abstract

This thesis aims to investigate possible correlations between charm production and baryon production in proton-proton collisions through three-particle correlations. The question attempted to be answered is where, for a given charmed baryon, the balancing anti-charm particle and balancing anti-baryon are located. The relative azimuthal angle $\Delta\phi$ and pseudorapidity $\Delta\eta$ between the trigger charmed baryon, light baryons and charmed mesons are calculated for different combinations of quantum numbers in the triplet of particles, using data simulated with the event generator Pythia8. Two different data sets are considered: forced charm production, in which each event starts with a primary hard scattering producing a $c\bar{c}$ pair back-to-back, and minimum bias. Two approaches are taken to answer the research question. Firstly, the balance function for the triplet of a trigger charmed baryon, light baryon with opposite baryon number to the trigger and charmed meson with opposite charm quantum number than the trigger is produced. This balance function is corrected for possible uncorrelated pairs and shows the true correlation between baryon number and charm quantum number conservation. Secondly, the baryon pair is restricted to a certain interval in momentum space and the effect on the charmed particle's placement is investigated. It is found that with forced charm production in place, the balancing charmed particle is produced back-to-back to the balancing baryon. The charmed hadrons are produced back-to-back in azimuthal angle and are uncorrelated in pseudorapidity. The baryons with opposite baryon number are found close to each other in momentum-space. In the more realistic case of minimum bias events, both the balancing baryon and balancing charmed particle follow each other and are found close to the triggering charmed baryon. These results can be understood when considering the production mechanisms used in the event generator.

Popular Science Summary

When ions are heated up to extreme temperatures they undergo a phase transition into so called quark-gluon plasma (QGP), an extraordinary type of matter in which the fundamental particles building up protons and neutrons move more or less freely. It is believed that the early universe was made up of this hot and dense mixture, so by studying the behaviour of this fluid we can learn more about how the building blocks of our universe were once formed. To understand the quark-gluon plasma, we must first understand the basic building blocks of matter. The fact that matter is made up of atoms and that these in turn consist of protons, neutrons and electrons is something most people learn about in high school. But in fact, protons and neutrons can be split into even smaller elementary particles called quarks. There are three pairs of quarks - up and down, strange and charm, and top and bottom. Protons are made up of one down and two up quarks, but more exotic particles are made up of other combinations of two or three of these quarks and their corresponding antiparticles.

When nuclei collide at very high energies, they can create conditions similar to those in the early universe. This is done at particle accelerators such as the Large Hadron Collider (LHC) at CERN, producing so called "little Bangs". The droplet of QGP which is formed in these collisions exists for a very short time, before decaying into showers of particles that are detected and analysed. Many theoretical predictions for properties of the QGP have been proposed and confirmed by experiments, such as the abundances and spatial distributions of the produced particles. However, recently signatures previously attributed to QGP were also found in proton-proton collisions. This was a big shock to the high-energy physics community since the QGP was not expected to form in collisions of smaller particles – there simply is not enough time. As researchers, we want to understand what is going on in these collisions and this thesis hopes to contribute to a small piece of this puzzle.

The particles produced in the collision are spread out in space around the collision point. By considering the relative positions of these particles, we can determine at what time in between collision and detection they are produced, which in turn gives clues about the production mechanisms, i.e. how they are produced. In this work, so called charmed particles are considered. These are exotic particles that include a charm (or anti-charm) quark and one or two other quarks, most often the up and down quarks. The proton-proton collisions are simulated using a model called Pythia, which is a Lund-based theoretical model often used in high-energy physics. It simulates the produced particles, their propagation towards the detectors and their decay into new particles. All of this information is in the analysis used to find the spatial distribution of the charmed particles in a so called three-particle correlation. In essence, this is a topological map which tells you the probability to find the protons and other charmed particles, if you have a charmed baryon at the origin. The results of this work may in future research be compared to experimental data to enable the evaluation of the theoretical models describing proton-proton collisions.

Acknowledgements

I would like to thank my supervisor, Alice Ohlson, for introducing me to particle physics way back at the beginning of my education and for giving me the opportunity to work on this bachelor project. Thank you for all the help and inspiration, for putting so much time and effort into this, and for always keeping your door open for questions. I would also like to thank all the other people whose expertise helped me along the way, especially Peter Christiansen and Christian Bierlich for the discussions of my results.

A special thanks to Mel, for all the long discussions, brainstorming and late nights coding. I would also like to thank the rest of my amazing friend group, Paul, Sora, Noah and Jordis, who wrote their thesis alongside me. You guys have made the last three years the best. I am also immensely grateful for the endless support from my parents, thank you for always believing in me. And lastly to fifteen-year-old me: I know you think you won't make it past twenty, but look at us now. I hope I have made you proud.

Contents

List of Acronyms

ALICE: A Large Ion Collider Experiment
BR: Branching Ratio
CERN: Conseil Européen pour la Recherche Nucléaire (European Council for Nuclear Research)
ECal: Electromagnetic Calorimeter
FC: Forced Charm
HCal: Hadronic Calorimeter
ITS: Inner Tracking System
LHC: Large Hadron Collider
MB: Minimum Bias
MC: Monte Carlo
PDG: Particle Data Group
QCD: Quantum Choromodynamics
QED: Quantum Electrodynamics
QGP: Quark-Gluon Plasma
RHIC: Relativistic Heavy-Ion Collider
SM: Standard Model
TOF: Time of Flight
TPC: Time Projection Chamber

1 Introduction

Particle collisions are one of the keystones in modern high energy physics, allowing us to probe the subatomic world by colliding highly energetic particles with each other and essentially backtracking the collision by detecting the particles produced. Proton-proton collisions are "simple" systems to investigate nuclear matter and are considered guides for more sophisticated processes such as nucleus-nucleus collisions. The strong coupling constant, which determines the interaction strength of the strong force, decreases with energy, so the physical nature of the proton-proton collisions varies with the energy scale. Hard interactions involving high energy transfer can be described by perturbative quantum chromodynamics (QCD). However, large contributions to particle production are the soft interactions, which are not described by perturbative QCD and demand other models. One of the most widely used models for the generation of high energy collision events in particle physics is the Lund-based Monte Carlo model Pythia8. Executing the program produces the final stage products of the collisions, including information such as particle type, momentum and multiplicity.

QCD is one of many areas of research in which there is a need for a constant interplay between theoretical models and experimental results and consequently, there is a clear need of defining observables to compare. This project will focus on quantum number production. More specifically, this project aims to investigate whether there is a correlation between the production of baryon number and the production of charm or not by probing the kinematics of charmed baryons, charmed mesons, and other light baryons produced in proton-proton collisions. Information about such dynamics is gathered by constructing so called three-particle correlation functions. This is done via the particles' relative azimuthal angle $\Delta\phi$ in the transverse plane and their relative longitudinal pseudorapidity $\Delta\eta$. In essence, we ask the question: if we produce a charmed baryon in a proton-proton collision, where are the balancing light baryon and the balancing charmed meson produced?

This project will produce a three-particle correlation between trigger charmed hadrons, charmed mesons with opposite charm quantum number than the trigger, and light baryons produced to conserve baryon number in the collision. Proton-proton collisions will be simulated using the Monte Carlo simulator Pythia 8.309 [1], both for forced hard production of $c\bar{c}$ quark pairs and minimum bias. The correlation function between charmed baryons, charmed mesons and light baryons is sensitive to the mechanisms of charm production, fragmentation and hadronisation. Therefore, investigating the correlations of these particles might give insight into when and where in the collision the charmed particles are found – both in relation to themselves and in relation to other baryons. This gives information about the dominant production mechanisms in the event generator. Arguably most importantly, measuring the correlation function of the charmed baryons, mesons, and light baryons using simulated data allows for future comparison with experimental data and can provide guidance on tuning the generators. Furthermore, the correlation function can possibly function as a signature of particle production in small systems. These studies are important not only for providing a better understanding of the underlying physics in proton-proton collisions but also for possible modifications of the interpretations of correlation functions in other high energy physics areas, such as heavy ion physics.

2 Theory

Before going into the details of this thesis, an introduction to particle physics and the Standard Model will be presented, followed by an overview of particle detection in the ALICE detector [2] and an outline of Pythia8, the event generator used to simulate the particles.

2.1 The Standard Model

The Standard Model of particle physics describes all known fundamental particles and three of the four forces in nature; the strong, the electromagnetic and the weak force. The particles building up matter, called fermions, include two groups named quarks and leptons. Each group consists of six particles and their corresponding antiparticles, which are related to each other in pairs, or "generations", ordered from lowest mass (and thus most stable) to highest mass (and least stable). All stable matter in the universe is made up of particles belonging to the first generation - "up quarks" and "down quarks". More exotic, unstable particles include quarks from the second generation, "strange quarks" and "charm quarks", and third generation, "top quarks" and "bottom quarks".

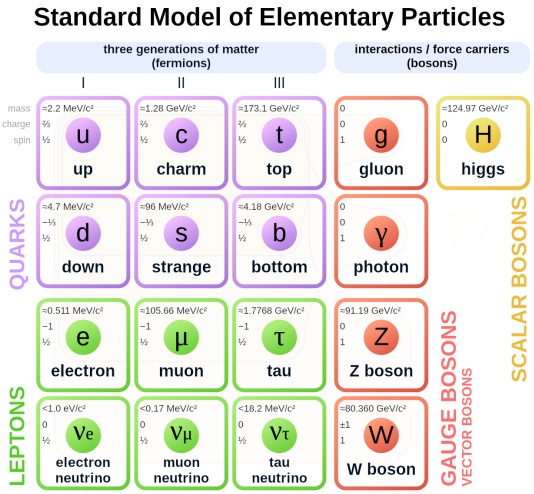

Figure 1: Schematic table of the particles in the Standard Model. Figure taken from [3].

In addition to the fermions, the Standard Model also includes four force carriers which are the particles giving rise to forces between other particles. These are the photon, the gluon, the Z-boson and the W-boson. The weak force is mediated by the W- and Z-bosons. These massive particles couple to all fermions, as well as to themselves. The electromagnetic and the weak force are described by a unified gauge theory called quantum electrodynamics (QED). At shorter distances (higher energies) both the electromagnetic and the weak interaction strength increase. Coupling constants which vary with energy scale are called running coupling constants, an effect which is even more important for the strong force coupling constant.

Nuclear matter is held together by the strong force, which is described by QCD and mediated by the gluon. As the name suggests, the strong force is the strongest of the forces. Gluons couple to so called "colour charge", an additional quantum number associated with quarks and gluons. Colour charge comes in three colours: red (r), green (g) and blue (b), and the corresponding anticolours. All particles seen in nature are colour-neutral, either in a triplet of all three colour charges (rgb) or as a doublet of colour and anticolour. As a result, there are two main groups of hadrons: baryons (qqq or $\overline{qqq}$) and

mesons ($q\overline{q}$). The gluon also carries colour-charge, namely a colour and an anti-colour, and can therefore self-interact. The larger the distance (lower energy), the more the gluon can self-interact and the stronger the interaction strength becomes. As a result, the force between quarks increases as they are pulled apart. In collider experiments, quarks are pulled apart with so much energy that showers of new particles are formed, called jets.

Elementary particles in the Standard Model carry many so called quantum numbers which are said to be intrinsic to them, such as spin, electric charge and lepton number. Quantum numbers describe values of conserved quantities in dynamical quantum systems, normally taking integer or half-integer numbers. The quantum numbers of interest in this thesis are the flavour charm and the baryon number. Charm, C, represents the difference between the number of charm quarks (n_c) and charm antiquarks ($n_{\overline{c}}$) present in a particle,

$$C = n_c - n_{\bar{c}}. \tag{1}$$

Charm is conserved in strong and electromagnetic interactions, but not in the weak interaction because of flavour mixing. Baryon number B is defined as

$$B = \frac{1}{3}(n_q - n_{\bar{q}}), \tag{2}$$

where n_q is the number of quarks and $n_{\bar{q}}$ the number of antiquarks. Particles with baryon number ± 1 are called baryons, while particles with baryon number 0 are called mesons. The baryon number is a strictly conserved quantum number, meaning that the sum of the baryon number of all incoming particles equals the sum of the baryon number of all outgoing particles resulting from a reaction [4].

Since this thesis focuses on the possible correlation between charm production and baryon production, the hadrons of special interest in this thesis are the charmed hadrons and light baryons. Some particle properties are listed in Table 1, 2 and 3. The Particle Data Group (PDG) numbering scheme is used as an identifier in particle generators such as Pythia and is taken from [5].

Particle	Antiparticle	Quarks	Mass [MeV/c^2]	C	B	Mean Lifetime [s]	Decays	PDG
Λ_c^+	Λ_c^-	udc	2286.46 ± 0.14	+1	+1	$(2.00 \pm 0.06) \times 10^{-13}$	$[p, K^-, \pi^+]$	4122
Ξ_c^+	Ξ_c^-	usc	2471.0 ± 0.4	+1	+1	$(4.42 \pm 0.26) \times 10^{-13}$	$[\Xi^-, 2\pi^+]$	4232
Ξ_c^0	$\overline{\Xi_c^0}$	dsc	2471.0 ± 0.4	+1	+1	$(1.12 \pm 0.13) \times 10^{-13}$	–	4132
Ω_c^0	$\overline{\Omega_c^0}$	ssc	2697.5 ± 2.6	+1	+1	$(268 \pm 24) \times 10^{-15}$	–	4332

Table 1: Charmed baryons used in analysis and some of their physical properties, namely antiparticle, quark content, mass, charm number, baryon number, mean lifetime, most common decay products and PDG code [6].

Particle	Antiparticle	Quarks	Mass [MeV/c^2]	C	B	Mean Lifetime	Decays	PDG
p	$\overline{p}$	uud	938.272	0	+1	$> 3.6 \times 10^{29}$ years	-	2212
n	$\overline{n}$	udd	939.565	0	+1	879.4 s	$p, e^-, \overline{\nu_e}$	2112

Table 2: Light baryons used in analysis and some of their physical properties [7] [8].

Particle	Antiparticle	Quarks	Mass [MeV/c^2]	C	B	Mean Lifetime [s]	Decays	PDG
D^0	$\overline{D^0}$	$c\overline{u}$	1864.84 ± 0.17	+1	0	$(1.040 \pm 0.007) \times 10^{-12}$	$[K, \mu, e, \pi]^{\pm}$	421
D^+	D^-	$c\overline{d}$	1869.62 ± 0.20	+1	0	$(4.101 \pm 0.015) \times 10^{-13}$	$[K, e, \pi]^{\pm}$	411
D_s^+	D_s^-	$c\overline{s}$	1968.47 ± 0.33	+1	0	$(5.00 \pm 0.07) \times 10^{-13}$	$[K, \pi]^{\pm}$	431

Table 3: Charmed mesons used in analysis and some of their physical properties [9] [10].

2.2 Small and Large System Collisions

The strong force and the mechanisms of QCD can be probed via particle collisions, by analysing the particles produced. These collisions range in scale from small systems, such as proton-proton collisions, to large system collisions, such as heavy-ion collisions. Scattering processes at high energy hadron colliders can be classified as either hard or soft, depending on the amount of momentum exchange between the interacting partons. Hard processes can be described using perturbative QCD to good precision, but perturbation theory fails to predict soft processes due to the large coupling constant, making the soft processes less well-understood. As a result of the large mass of the charm quark, they are produced in hard processes, visualised in Figure 2. Production of lighter quarks, such as up and down quarks, are mainly produced in soft processes. Although the understanding of QCD and its production mechanisms in different collision systems has increased drastically over the past decades, there are still many unanswered questions.

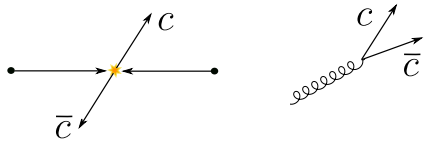

Figure 2: Left: Production of $c\overline{c}$ pair as a result of initial head on interactions. Since the momentum in the lab frame is zero, the quark pair is produced back-to-back. Right: Production of $c\overline{c}$ pair as a result of gluon pair production. Since the gluon has a forward momentum in the lab frame, the quark pair is also boosted in the lab frame and more likely to be in close proximity to each other.

In 2001, early results from the Relativistic Heavy-Ion Collider (RHIC) indicated that in head-on lead-lead collisions the majority of the collision energy was deposited into a medium whose expansion was well described by relativistic hydrodynamics. Further experiments showed that this exotic state of matter, called the quark-gluon plasma (QGP), had a very low viscosity, a temperature of around four trillion Kelvin and is composed of deconfined quarks. The standard description of these large system collisions has been tested with great detail and many signatures of the QGP such as radial and anisotropic flow and associated flow coefficients v_n, jet quenching and strangeness enhancement have been found [11]. However, signatures previously attributed solely to the QGP have also been found in smaller systems – mainly collective behaviour and strangeness enhancement [12] [13]. This is puzzling since the lifetime of the system formed in these collisions should be too short to undergo any phase transition necessary to produce QGP. This begs the question of whether our current understanding of large systems is incorrect, or if the descriptions of smaller systems are incomplete. Whatever the answer, it highlights the importance of further understanding small system collisions and the basic properties of QCD [14].

2.3 Particle Detection

Large collision systems are the main object of study for the heavy-ion detector ALICE (A Large Ion Collider Experiment) at CERN, which focuses on the strong interaction sector of the Standard Model. Its main objective is to detect the particles produced in heavy ion collisions, but comprehensive data is taken during proton-proton runs as reference data for the heavy-ion program. Particles are identified by the characteristic signatures they leave in the detector, consisting of a set of components stacked in layers around the collision point. The main tracking system of ALICE is the inner tracking system (ITS) and the time projection chamber (TPC), which together are able to record most charged particles traversing it and identifying them through means such as specific ionisation energy loss and time of flight (TOF) measurements. Neutral particles can be reconstructed through their decay products [2].

Even though this thesis is based on simulated data, it is for future purposes still interesting to consider how the particles of interest would be detected with the ALICE detector. The Λ_c^+ decays as $\Lambda_c^+ \longrightarrow pK^-\pi^+$ with branching ratio (BR) $(6.35 \pm 0.33)\%$, $\Lambda_c^+ \longrightarrow pK_s^0$ with BR= $(1.58 \pm 0.08)\%$, and $\Lambda_c^+ \longrightarrow e^+\mu_e\Lambda$ with BR= $(3.8 \pm 0.4)\%$. The K_s^0 decays into pions and the Λ into a proton and a pion. The charged tracks in these decays are reconstructed using the central barrel detectors. The neutral K_S^0 and Λ are identified based on the V-shaped decay topology. The identification of pions, kaons, protons and electrons is based on the specific energy loss dE/dx in the TPC detector and time of flight measurements [15]. D mesons are identified via the decay channels $D^0 \longrightarrow K^-\pi^+$ with BR= $(3.89 \pm 0.04)\%$, $D^+ \longrightarrow K^-\pi^+\pi^+$ with BR= $(8.98 \pm 0.28)\%$ and $D_s^0 \longrightarrow \phi\pi^+ \longrightarrow K^+K^-\pi^+$ with BR= $(2.27 \pm 0.08)\%$ [16].

The coordinates used to describe the direction of a track in particle collisions are the azimuthal angle ϕ and the Lorentz invariant pseudorapidity η as seen in Figure 3. The pseudorapidity is related to the longitudinal angle θ of the three-momentum to the beam-line through

$$\eta = -\ln\left(\tan\left(\frac{\theta}{2}\right)\right). \tag{3}$$

Particles travelling parallel to the beam have pseudorapidity $\eta = \pm\infty$, while trajectories perpendicular to the beam have pseudorapidity $\eta = 0$. The ALICE central barrel detector has a pseudorapidity range of $|\eta| < 0.88$ [2]. The azimuthal angle ϕ is the polar angle in the x-y plane perpendicular to the beam axis. The origin is chosen arbitrarily, but in simulations it is usually chosen to be in the same direction as the leading track and thus changes from event to event. The azimuthal plane is divided into three regions. The toward side is $\phi \in [-\pi/3,\ \pi/3]$, the away side $\phi \in [2\pi/3,\ 4\pi/3]$, and the traverse region $\phi \in [\pi/3,\ 2\pi/3]$ and $\phi \in [4\pi/3,\ 5\pi/3]$.

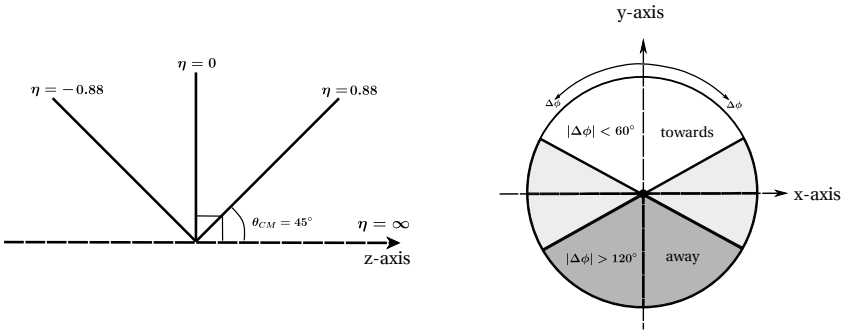

Figure 3: Left: The pseudorapidity η. The z-axis is along the beamline and θ_{CM} is the centre of mass scattering angle. Right: The azimuthal angle ϕ.

2.4 Particle Correlations

Information concerning collectivity, which in itself has been considered a signature of QGP, can be gathered through measuring particle correlations, often parametrised via the particles' relative angle $\Delta\phi = \phi_1 - \phi_2$ and $\Delta\eta = \eta_1 - \eta_2$. Some examples of correlations include hadronic resonances giving rise to two-particle correlations, hard scattering of partons from incoming hadrons resulting in jets, and low momentum transfer scattering resulting in long-range correlations in pseudorapidity as a consequence of momentum conservation [14]. These correlation functions are sensitive to production mechanisms and are therefore a useful tool when probing QCD.

A two-particle correlation function $C^{(2)}$ is defined as

$$C^{(2)}(\Delta\eta, \Delta\phi) = \frac{1}{N_{\text{pairs}}} \frac{d^2 N_{\text{pairs}}}{d\Delta\eta d\Delta\phi} \tag{4}$$

where $\Delta\eta$ and $\Delta\phi$ are the differences in pseudorapidity and azimuthal angle respectively between the trigger particle and the associated particle, and N_{pairs} the number of trigger associated pairs. In this thesis, the correlation function is normalised with respect to the number of triggers, N_{trig}, giving the associated yields per trigger

$$C^{(2)}(\Delta\eta, \Delta\phi) = \frac{1}{N_{\text{trig}}} \frac{d^2 N_{\text{pairs}}}{d\Delta\eta d\Delta\phi}. \tag{5}$$

Two-particle correlations are a well-used tool in particle physics. This can be expanded to three-particle correlations, $C^{(3)}$, given by

$$C^{(3)}(\Delta\eta_{1,2}, \Delta\eta_{1,3}, \Delta\phi_{1,2}, \Delta\phi_{1,3}) = \frac{1}{N_{\text{trig}}} \frac{d^4 N_{\text{triplets}}}{d\Delta\phi_{1,2} d\Delta\phi_{1,3} d\Delta\eta_{1,2} d\Delta\eta_{1,3}}. \tag{6}$$

where 1 denotes the first trigger particle and 2 and 3 are the two other particles in the triplet [17]. In this thesis, particle 1 corresponds to the charmed baryon, particle 2 is the light baryon and particle 3 is the charmed meson. Using this definition, correlation functions for different combinations of charm quantum number and baryon quantum number will be created, to produce a so called balance function [18]. This is explained more in detail in section 3.

2.5 Pythia

The data used to produce the three-particle correlations in this thesis is simulated using the Monte Carlo event generator Pythia8. In a simplified explanation, one can say that the event starts with two initial particle beams approaching each other. When the particles collide, partons interact with each other over a variety of energy scales through both hard and soft processes, producing new partons. These branch into final state parton showers. Because of the non-perturbative nature of QCD, it is not possible to derive the hadronic parton distributions from first principle, so an interplay between theory and experimental data is vital for the parametrisations. The colour-charged partons are converted into colour-neutral hadrons in a process called hadronisation. In Pythia, these fragmentations are modeled as so called string fragmentation. The model describes the linear confinement of the colour singlet $q\overline{q}$ jet as a massless, one-dimensional string. As the distance increases, the tension in the string increases to a point in which it breaks and a new $q\overline{q}$ pair(s) are produced. If the quark pair has a transverse mass, they cannot be produced in the same point and need to tunnel through a forbidden region. This tunnelling probability is given by

$$\frac{1}{\kappa}\frac{d\mathcal{P}}{d^2p_\perp} \propto \exp(-\pi m_\perp^2/\kappa) = \exp(-\pi m^2/\kappa)\exp(-\pi p_\perp^2/\kappa), \tag{7}$$

where $m_\perp$ is the traverse mass of the quark, κ the string tension and $p_\perp$ the traverse momentum. The non-zero mass suppression is viewed as a free parameter and tuned to data. Using this, one can see that in string breaking processes the production of charm compared to up and down quarks is suppressed by a factor of

$$\exp(-\pi(m_c^2 - m_{ud}^2)/\kappa) \approx 10^{-11}. \tag{8}$$

The string-breaking producing the triplet Λ_C, $\overline{p}$ and $\overline{D^0}$ is shown in Figure 4 [1].

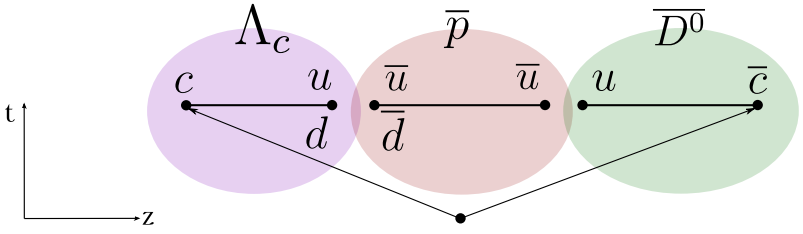

Figure 4: Schematic illustration of one possible way the strings break to produce a Λ_c, $\overline{p}$ and $\overline{D^0}$, where the $c\overline{c}$ pair have been produced through hard processes.

3 Method

Before describing the method used in this work, it is necessary to present a note on the particles used in the analysis and introduce some notation regarding them. To increase the statistics, we look at all triplets of charmed baryons, light baryons and charmed mesons. Most of these are $\Lambda_c^+(\Lambda_c^-)$, $D^0(\overline{D^0})$ and protons or neutrons but other particles, as listed in Tables 1, 2 and 3, are also included. To simplify, a more concise notation is used as explained in Table 4 below.

Notation	Explanation
Λ	All charmed baryons (see table 1), with charm number +1 or -1 and baryon number +1 or -1. These are the triggering particles.
p	All light baryons (see table 2) with the same baryon number as the associated triggering charmed baryon.
$\overline{p}$	All light baryons with the opposite baryon number as the associated triggering charmed baryon.
D	All charmed mesons (see table 3) with the same charm number as the associated triggering charmed baryon.
$\overline{D}$	All charmed mesons with the opposite charm number as the associated triggering charmed baryon.

Table 4: Notation for the particles used henceforth.

3.1 Particle Generation

3.1.1 Pythia

The particles used for the analysis of this work are produced using the Monte Carlo simulator Pythia 8.309, which is described in more detail in section 2.4. When running the simulation, a number of conditions are placed on the production. Namely,

```
pythia.readString("HardQCD:gg2ccbar = on");
pythia.readString("HardQCD:qqbar2ccbar = on");
pythia.readString("ParticleDecays:limitTau0 = on");
pythia.readString("ParticleDecays:tau0Max = 0");
```

where the two first lines force a $c\overline{c}$ production back-to-back in the primary hard scattering, and the last two lines ensure that the charmed baryons do not decay weakly. A set of data is also produced with minimum bias, where the heavy quark pair is not forced to be produced in the primary hard scattering. The ALICE central barrel detector has a pseudorapidity range of $|\eta| < 0.88$. This restriction is not relevant when simulating particles, but to make future comparison of results easier, the restriction $|\eta| \leq 1$ is placed on the simulated particles. Before an event is saved to a separate file, it is checked to ensure that it includes at least one charmed baryon, one charmed meson and one light baryon. The multiplicity of the events for the forced charm production and minimum bias is shown in Figure 5, showing that if the $c\overline{c}$ production is not forced in the primary hard scattering, it happens at higher multiplicities.

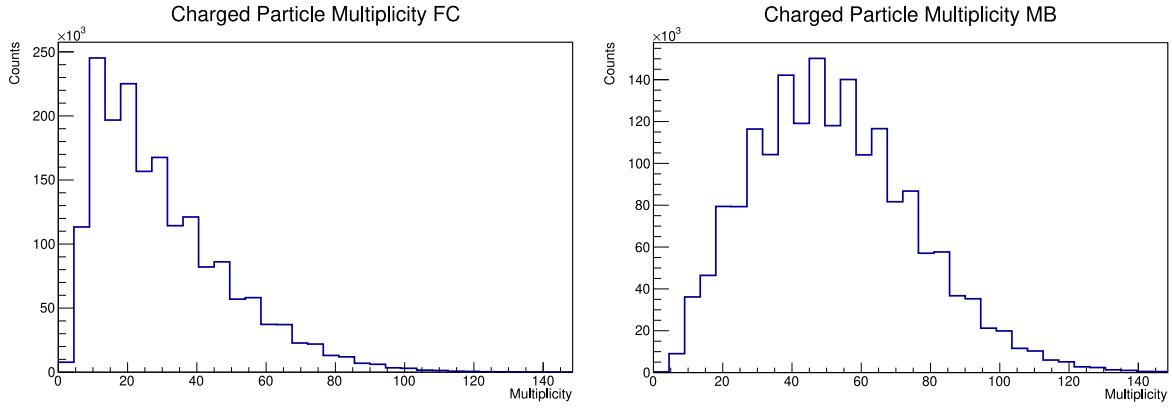

Figure 5: Left: Multiplicity of the events for the forced charm (FC) production. Right: Multiplicity of the events in the minimum bias (MB) case.

3.1.2 Toy Model

A simple toy model for particle production was constructed using a pseudo-random number generator. In each event, a fraction of the particles were assigned η and ϕ randomly in the chosen intervals $|\eta| \leq 1$ and $\phi \in [0, 2\pi]$. Half of the remaining particles in the event were given a random η and ϕ within Gaussian distributions centred at some random η_1 and ϕ_1 respectively, and $\sigma = 0.1$. The rest of the particles were set η and ϕ from Gaussian distributions centred at $\phi_2 = \phi_1 + \pi$ and a random η_2 to simulate back-to-back jets. A possibility of assigning each particle an identifying integer was included, to separate between "different" particles. The toy model was then used to test out two- and three-particle correlations. The balance function, which will be explained shortly, was also tested using the toy model to ensure that it showed no correlation when none were simulated.

3.2 Correlation Functions

The analysis is done in C++, using the ROOT framework [19]. To construct the correlation functions between charmed baryons, charmed mesons and light baryons, $\Delta\eta$ and $\Delta\phi$ between the particles in each triplet are calculated. The charmed baryon is chosen as the trigger particle, such that for each charmed baryon the azimuthal angle and pseudorapidity to all charmed mesons and light baryons within the same event is determined. In total, four correlations for different combinations of quantum numbers in the triplet are constructed: opposite baryon number and opposite charm C_1, opposite baryon number and same charm C_2, same baryon number and opposite charm C_3, and finally same baryon number and same charm C_4. Each of these is assigned a four-dimensional histogram (THn), which is filled with $(\Delta\phi_{\Lambda,p(\overline{p})}, \Delta\phi_{\Lambda,D(\overline{D})}, \Delta\eta_{\Lambda,p(\overline{p})}, \Delta\eta_{\Lambda,D(\overline{D})})$ depending on the combinations of the quantum numbers of Λ, $p(\overline{p})$ and $D(\overline{D})$. Rotational symmetry for the azimuthal angle is ensured by adding or removing 2π from $\Delta\phi$ if it is outside of the chosen range $[-\pi/2,\ 3\pi/2]$.

As a result of the acceptance range in η, the correlation functions will showcase a symmetric background behaviour. For a one-dimensional case, this would look like a triangle centered at the origin and stems from the fact that there will be significantly more particles with $\Delta\eta = 0$ than $\Delta\eta = 2$. To see signals which are only due to inherent correlations between particles, this acceptance factor needs to be removed. In practice, this is done by considering correlations between particles which are completely uncorrelated – the only "signal" in this correlation function is that of the acceptance. To do so, the triggering charmed baryons are correlated to charmed mesons and light baryons produced in the ten prior events. These are called "mixed event correlations" and are normalised in such a way that the probability for a triplet of particles being close to each other is unity, which means that they are normalised with respect to $(\Delta\phi_{\Lambda,p}, \Delta\phi_{\Lambda,D}, \Delta\eta_{\Lambda,p}, \Delta\eta_{\Lambda,D}) = (0, 0, 0, 0)$. The correlation functions of particles within one event are divided by the mixed event correlations to obtain what henceforth is called "signal correlation functions", which is visualised in Figure 6. In order to produce the actual correlation functions

$$C_n^{(3)}(\Delta\phi_{\Lambda,p}, \Delta\phi_{\Lambda,D}, \Delta\eta_{\Lambda,p}, \Delta\eta_{\Lambda,D}) = \frac{1}{N_{\text{trig}}} \frac{d^4N}{d\Delta\phi_{\Lambda,p} d\Delta\phi_{\Lambda,D} d\Delta\eta_{\Lambda,p} d\Delta\eta_{\Lambda,D}}, \tag{9}$$

the histograms are scaled with the total number of triggers, N_Λ, and the binwidths of the histogram. These four-dimensional objects are projected on two of the four axes in order to visualise the results, using the "Projection" command defined for THn ROOT

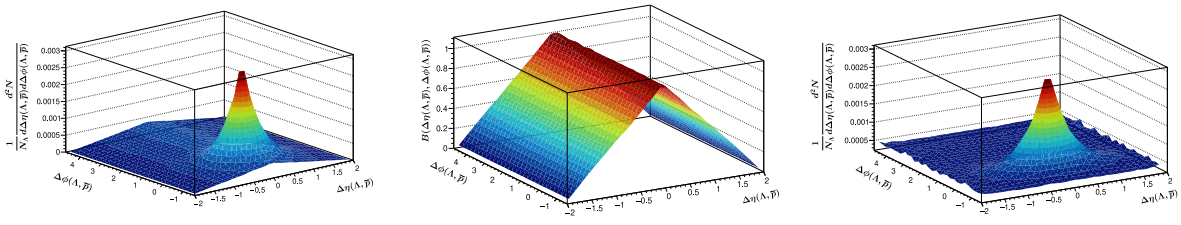

Figure 6: Left: Same-event two-particle correlation function for charmed baryons and light baryons with opposite baryon number. Middle: The acceptance, which is the correlation of particles from mixed events, $B(\Delta\eta(\Lambda,\overline{p}),\Delta\phi(\Lambda,\overline{p}))$ normalised to one. Right: The same-event two-particle correlation function after correcting for the acceptance by dividing the left plot by the middle plot.

objects and scaling with the binwidth of the axis not projected over. This produces four projected signal correlation functions for each of the four signal correlation functions:

$$C_n^{(3)}(\Delta\phi_{\Lambda,p}\Delta\eta_{\Lambda,p}) = \frac{1}{N_{\text{trig}}}\frac{d^2N}{d\Delta\phi_{\Lambda,p}d\Delta\eta_{\Lambda,p}} = \frac{1}{N_{\text{trig}}}\int \frac{d^4N}{d\Delta\phi_{\Lambda,p}d\Delta\phi_{\Lambda,D}d\Delta\eta_{\Lambda,p}d\Delta\eta_{\Lambda,D}} d\Delta\eta_{\Lambda,D}d\Delta\phi_{\Lambda,D} \tag{10}$$

$$C_n^{(3)}(\Delta\phi_{\Lambda,D}\Delta\eta_{\Lambda,D}) = \frac{1}{N_{\text{trig}}}\frac{d^2N}{d\Delta\phi_{\Lambda,D}d\Delta\eta_{\Lambda,D}} = \frac{1}{N_{\text{trig}}}\int \frac{d^4N}{d\Delta\phi_{\Lambda,p}d\Delta\phi_{\Lambda,D}d\Delta\eta_{\Lambda,p}d\Delta\eta_{\Lambda,D}} d\Delta\eta_{\Lambda,p}d\Delta\phi_{\Lambda,p} \tag{11}$$

$$C_n^{(3)}(\Delta\phi_{\Lambda,p}\Delta\phi_{\Lambda,D}) = \frac{1}{N_{\text{trig}}}\frac{d^2N}{d\Delta\phi_{\Lambda,p}d\Delta\eta_{\Lambda,p}} = \frac{1}{N_{\text{trig}}}\int \frac{d^4N}{d\Delta\phi_{\Lambda,p}d\Delta\phi_{\Lambda,D}d\Delta\eta_{\Lambda,p}d\Delta\eta_{\Lambda,D}} d\Delta\eta_{\Lambda,D}d\Delta\eta_{\Lambda,p} \tag{12}$$

$$C_n^{(3)}(\Delta\eta_{\Lambda,p}\Delta\eta_{\Lambda,D}) = \frac{1}{N_{\text{trig}}}\frac{d^2N}{d\Delta\eta_{\Lambda,p}d\Delta\eta_{\Lambda,D}} = \frac{1}{N_{\text{trig}}}\int \frac{d^4N}{d\Delta\phi_{\Lambda,p}d\Delta\phi_{\Lambda,D}d\Delta\eta_{\Lambda,p}d\Delta\eta_{\Lambda,D}} d\Delta\phi_{\Lambda,p}d\Delta\phi_{\Lambda,D}. \tag{13}$$

The correlation functions can be looked at from two different perspectives; the magnitude and the shape. In general, the overall shape informs about the relative strengths of the different production mechanisms, while the magnitude depends on the combined strength of said production mechanisms.

3.3 Balance Function

Next, the balance function is created. This is the "true" three-particle correlation function representing the balanced particle triplet, corrected for the possible two-particle correlation between only the charmed baryon and light baryon, or charmed baryon and charmed meson. This correlation function shows where the Λ, $\overline{p}$ are compared to the Λ, $\overline{D}$ (as well as the corresponding charge conjugates). The balance function is constructed as follows:

$$C_{\text{balance}} = C_1 - C_2 - C_3 + C_4. \tag{14}$$

The correlation needs to be corrected for random combinations, that is, particles produced in different interactions where the correlation is not between all particles within the triplet. To remove any random combinations of charmed baryons and charmed mesons with opposite charm quantum number, the correlation of charmed baryons and charmed

mesons with the same charm quantum number, C_2, is subtracted. Note that this builds on the assumption that random pairs of Λ and $\overline{D}$ (and the charge conjugates) behave the same way as pairs of Λ and D (and the charge conjugates) since these do not conserve charm quantum number. For weak interactions, all four correlations will have the same probability, but in strong interactions – which is what we are interested in – we can say that particle pairs with the same charm quantum number ought to be comparable to uncorrelated particle pairs with opposite charm quantum number, produced in different interactions. Similarly, random pairs of charmed and light baryons with opposite baryon numbers are removed by subtracting the correlation function of the same baryon number and opposite charm quantum number, C_3. At this point, the same baryon number and same charm have been removed one too many times since C_2 and C_3 both include triplet in which all three particles are uncorrelated, which is corrected for by adding the correlation function corresponding to these triplets, C_4, back in. The projection procedure described earlier is applied to the balance function, such that four two-dimensional histograms are produced.

3.4 Ranges

In addition to the balance function, the possible correlation between baryon number and charm quantum number is investigated by only considering $\Delta\phi_{\Lambda,p(\overline{p})}$ and $\Delta\eta_{\Lambda,p(\overline{p})}$ in a fixed range. On the four-dimensional signal correlation functions, a range is set on axis 0 and 2, corresponding to $\Delta\phi_{\Lambda,p(\overline{p})}$ and $\Delta\eta_{\Lambda,p(\overline{p})}$. Four different ranges are considered:

$$\begin{array}{llll} (1): & |\Delta\phi_{\Lambda,p(\overline{p})}| < 0.3, & |\Delta\eta_{\Lambda,p(\overline{p})}| < 0.2 & (3): \quad |\Delta\phi_{\Lambda,p(\overline{p})} - \pi| < 0.3, \quad |\Delta\eta_{\Lambda,p(\overline{p})}| < 0.2 \\ (2): & |\Delta\phi_{\Lambda,p(\overline{p})}| < 0.3, & |\Delta\eta_{\Lambda,p(\overline{p})}| \leq 2 & (4): \quad |\Delta\phi_{\Lambda,p(\overline{p})} - \pi| < 0.3, \quad |\Delta\eta_{\Lambda,p(\overline{p})}| \leq 2. \end{array}$$

The ranges are implemented by using the function "SetRangeUser". The four-dimensional correlation functions are produced and projected in the same manner as described earlier but divided by a different trigger, namely $N^{(x)}_{\Lambda,p(\overline{p})}$ as described in Table 5. The same is done for the signal correlation functions without a set range, where the trigger is instead $N_{\Lambda,p(\overline{p})}$. Using these triggers, the correlation functions will show the number of associated charmed mesons per light baryon and charmed baryon pair, relative to the position of the charmed baryon. The signal correlation functions with a set range are divided by the signal correlation functions without a set range. This fraction is in turn projected onto $\Delta\phi_{\Lambda,D(\overline{D})}$ and for each of the four ranges, all four correlations are plotted in the same plot so that the overall shapes of the fractions are comparable.

3.5 Triggering

Below, an explanation and numerical value are given to all the triggers used in the analysis, both for the forced charm production and minimum bias.

Notation	Explanation	Value FC	Value MB
N_{Λ}	All charmed baryons produced in the events.	14347194	4847221
$N_{\Lambda,p(\overline{p})}$	All pairs of charmed baryons and light baryons with the same (or opposite) baryon number produced in the event.	4044910 (8149890)	4766760 (6697598)
$N^{(1)}_{\Lambda,p(\overline{p})}$	All pairs of charmed baryons and light baryons with the same (or opposite) baryon number, within range (1).	66622 (559278)	77065 (382161)
$N^{(2)}_{\Lambda,p(\overline{p})}$	All pairs of charmed baryons and light baryons with the same (or opposite) baryon number, within range (2).	363731 (1782233)	419901 (1185115)
$N^{(3)}_{\Lambda,p(\overline{p})}$	All pairs of charmed baryons and light baryons with the same (or opposite) baryon number, within range (3).	77165 (90194)	93861 (98740)
$N^{(4)}_{\Lambda,p(\overline{p})}$	All pairs of charmed baryons and light baryons with the same (or opposite) baryon number, within range (4).	414581 (490868)	500659 (525684)

Table 5: Explanation of the triggers used in the analysis. These were counted during the particle generation of Pythia and are therefore each particle or pair is not necessarily part of an analysed triplet.

4 Results and Discussion

Next, the results of the analysis are presented and discussed. The results are obtained by analysing all particles listed in Tables 1, 2 and 3, but the analysis was also run on triplets only consisting of Λ_c^+, D^0 and p (and the corresponding antiparticles). This did not change the results visibly, other than decreasing the size of the data set. The projections of the correlation functions are notated as $C(\Delta\phi_{\Lambda,p(\overline{p})}, \Delta\phi_{\Lambda,D(\overline{D})})$, where

$$C(\Delta\phi_{\Lambda,p(\overline{p})}, \Delta\phi_{\Lambda,D(\overline{D})}) = \frac{1}{N_{\Lambda}} \frac{d^2N}{d\Delta\phi_{\Lambda,p(\overline{p})} d\Delta\phi_{\Lambda,D(\overline{D})}}, \tag{15}$$

The same goes for the other projections, as defined in equation (10)-(13). As a result of the triggering used, the amplitude of these three-particle correlations describes the number of times a triplet is found within the given coordinates for any $\Lambda(\bar{\Lambda})$ in the event. The one-dimensional correlation function used for the ranges is notated as $C(\Delta\phi_{\Lambda,D(\overline{D})})$, where

$$C(\Delta\phi_{\Lambda,D(\overline{D})}) = \frac{1}{N_{\Lambda,p(\overline{p})}} \frac{dN}{d\Delta\phi_{\Lambda,D(\overline{D})}}. \tag{16}$$

The triggers for the ranges are done with respect to particle pairs, as described in Table 5. All plots presented are projections of the four-dimensional three-particle correlation functions.

4.1 Correlation Functions Forced Charm Production

Firstly, a qualitative discussion of the four separate correlation functions is presented. In this section, only a certain subset of the projections are shown, but the remaining figures can be found in the Appendix. In general, with the forced charm production active in the particle generation, the charmed baryon and charmed meson with opposite charm number are found back-to-back, while the charmed baryon and light baryon with opposite baryon number are found in the same jet peak, near in phase space. For the same baryon number, it tends to be disfavoured for the charmed baryon and light baryon to be produced close to each other. The same goes for the same charm number.

4.1.1 Projection on $\Delta\phi_{\Lambda,p(\overline{p})}$ and $\Delta\phi_{\Lambda,D(\overline{D})}$

Figure 7 shows the four different correlation functions projected on $\Delta\phi_{\Lambda,p(\overline{p})}$, $\Delta\phi_{\Lambda,D(\overline{D})}$.

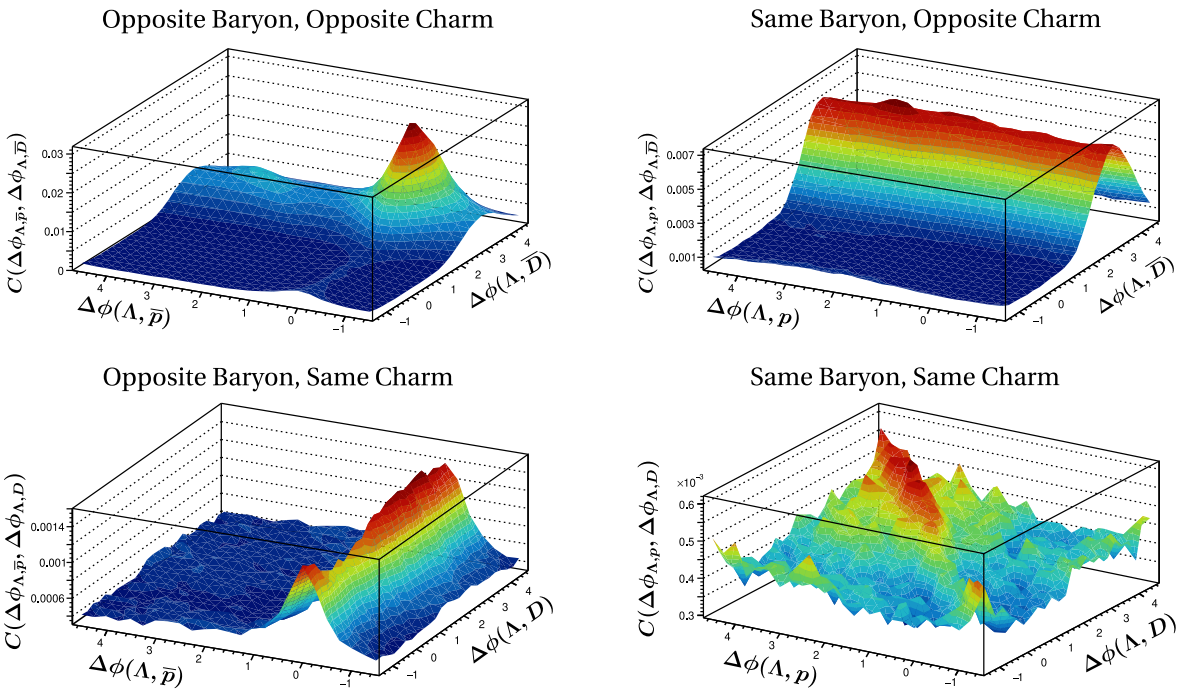

Figure 7: Correlation functions projected on $\Delta\phi_{\Lambda,p(\overline{p})}$, $\Delta\phi_{\Lambda,D(\overline{D})}$ for the four different combinations of baryon and charm number. Λ, D and p are as defined in Table 4.

The correlation function for the opposite baryon number, opposite charm, is shown in the upper left corner of Figure 7. We can see a clear peak at $(\Delta\phi_{\Lambda,\overline{p}}, \Delta\phi_{\Lambda,\overline{D}}) = (0, \pi)$, showing that the baryon and meson with opposite charm quantum number are mainly produced back-to-back, while the particles with opposite baryon number, i.e. the charmed baryon and the proton or neutron, are produced close together in the azimuthal angle. There is also a smaller peak around $(\Delta\phi_{\Lambda,\overline{p}}, \Delta\phi_{\Lambda,\overline{D}}) = (\pi, \pi)$, showing the situation in which the compensating charmed meson and baryon are both produced back-to-back to the triggering charmed baryon.

In the lower left corner of Figure 7, the same projection of the four-dimensional object is shown for the correlation of the opposite baryon number and same charm. Similarly to the opposite baryon opposite charm correlation function, the particles with balancing baryon number are close together. The charmed hadrons are distributed in $\Delta\phi$, with a disfavouring of being close together.

In the upper right corner of Figure 7, the correlation function for the same baryon number and opposite charm is shown, dominated by the initial forced production of $c\bar{c}$ pair back-to-back, while the charmed baryon and light baryon do not seem to, in this triplet, favour any particular placement.

Lastly, the same baryon number same charm correlation is shown in the lower right

corner of Figure 7. Here we can see that $\Delta\phi_{\Lambda,D} \approx \Delta\phi_{\Lambda,p}$ is favoured, while $\Delta\phi_{\Lambda,p} = 0$ and $\Delta\phi_{\Lambda,D} = 0$ is disfavoured. This can be understood with the argument that it is hard to produce a triplet with the same charm and same baryon number in close proximity to each other since this demands more particle production to balance the quantum numbers, and thus more energy.

4.1.2 Projection on $\Delta\eta_{\Lambda,p(\overline{p})}$ and $\Delta\eta_{\Lambda,D(\overline{D})}$

Figure 8 shows the correlation functions projected on $\Delta\eta_{\Lambda,p(\overline{p})}$ and $\Delta\eta_{\Lambda,D(\overline{D})}$, complementing the discussion above.

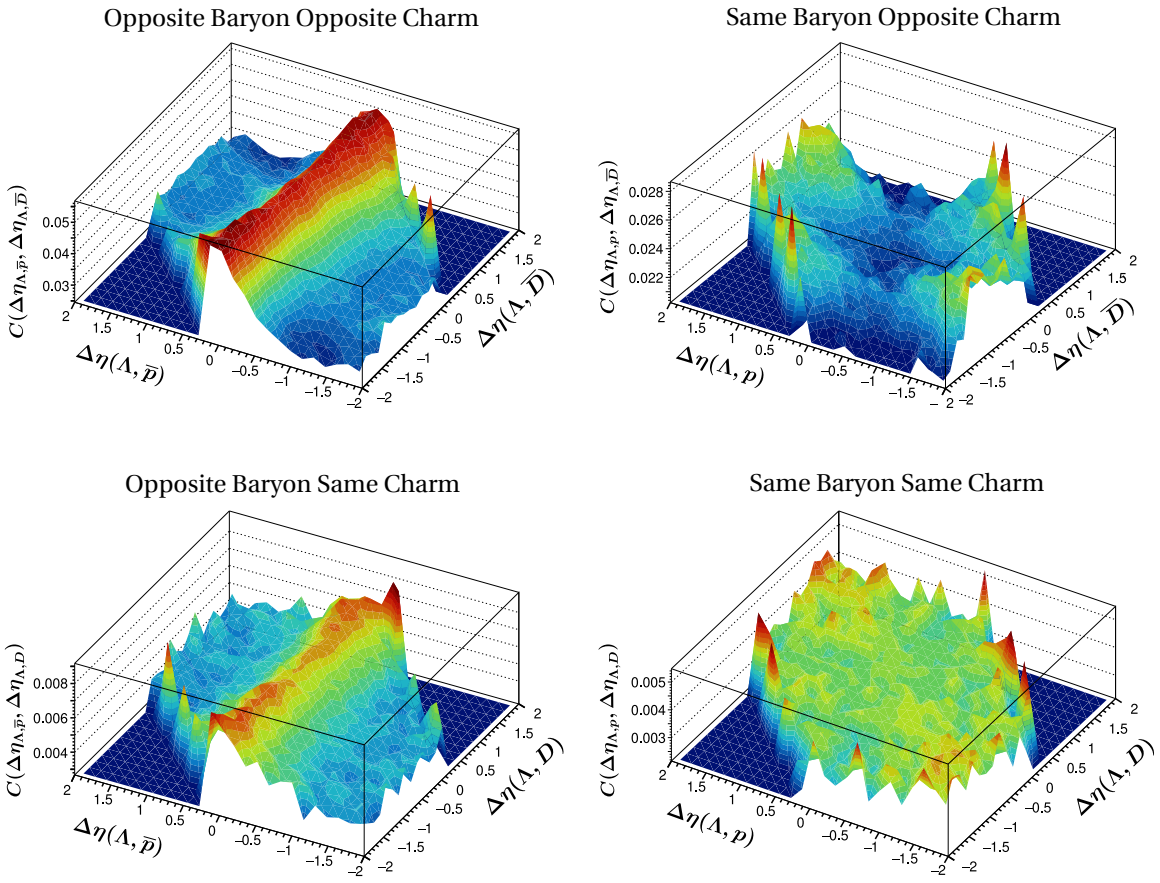

Figure 8: Correlation functions projected on $\Delta\eta_{\Lambda,p(\overline{p})}$, $\Delta\eta_{\Lambda,D(\overline{D})}$ for the four different combinations of quantum numbers, using the forced charm production.

In the upper left corner of Figure 8 the projection on pseudorapidity for the correlation function of opposite baryon opposite charm is shown. For the opposite baryon opposite charm, we see that the baryons are produced close to each other in pseudorapidity, while the charmed hadrons do not seem to favour any particular $\Delta\eta$.

In the lower left corner of Figure 8, the same projection is shown for the correlation of opposite baryon number and same charm. Similar behaviour as in the opposite baryon opposite charm can be seen in this triplet, although less prominent. It seems to be disfavoured for the charmed hadrons to be produced close to each other.

In the upper right corner of Figure 8 the correlation function for the same baryon opposite

charm triplets is shown. The baryons with the same baryon number are disfavoured to be in close proximity, while the charmed hadrons again do not show much preference.

Lastly, the same baryon same charm correlation function projected on $\Delta\eta_{\Lambda,p}$, $\Delta\eta_{\Lambda,D}$ is shown in the lower right corner of Figure 8. This correlation function shows no clear correlations.

4.1.3 Discussion

To summarise the correlation functions for the different combinations of quantum numbers, we can see that opposite baryon number particles show a tendency to be close to each other in momentum-space, while the same baryon number particles showcase an anti-correlation near each other. This can most clearly be seen in the projections of the correlation functions over pseudorapidity. The charmed hadrons with opposite charm are located back-to-back in azimuthal angle but distributed in pseudorapidity, indicating that the initial hard scattering is the main production mechanism of charm quarks. The same charm particles are either uncorrelated or show an aversion to closeness. It should be noted that the amplitudes of these four correlation functions presented vary drastically, with the opposite baryon number opposite charm having substantially more counts than the three others, reiterating why this is the combination of quantum numbers we are mostly interested in when looking for possible correlations. The correlation functions with the same charm particles have the lowest amplitude and the least amount of statistics, as this is a heavily suppressed production. The correlation functions presented above also include triplets in which there is no correlation between all three particles. It is therefore not possible to with certainty know which production mechanisms is the most dominant, which is why we need the balance function (see section 4.3).

4.2 Correlation Functions Minimum Bias

Next, the correlation functions for the minimum bias data, in which not every event starts initially producing a $c\bar{c}$ pair back-to-back, are presented in a similar manner. Compared to the forced charm production, in the minimum bias the distribution of charmed baryons and charmed mesons changes significantly while the distribution of charmed baryons and light baryons stays practically the same. It is still unfavoured to produce the same baryon number or charm close together in phase space and the opposite baryon number particles are still produced within the same jet peak. The opposite charmed meson is now instead produced in close proximity to the charmed baryon. This mainly affects the correlations functions in which the charmed hadrons have opposite charm number.

4.2.1 Projection on $\Delta\phi_{\Lambda,p(\overline{p})}$ and $\Delta\phi_{\Lambda,D(\overline{D})}$

Below, the projection on $\Delta\phi_{\Lambda,p(\overline{p})}$, $\Delta\phi_{\Lambda,D(\overline{D})}$ of the four correlation functions for minimum bias is shown.

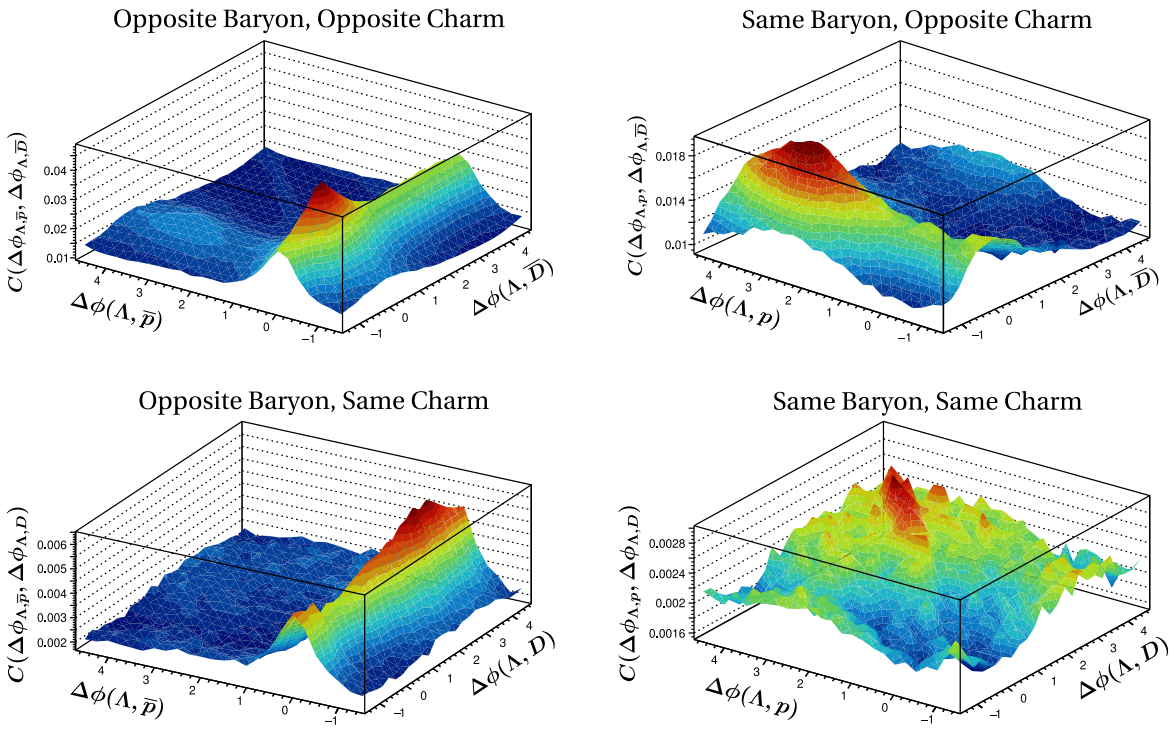

Figure 9: Correlation functions projected on $\Delta\phi_{\Lambda,p(\overline{p})}$, $\Delta\phi_{\Lambda,D(\overline{D})}$ for the different combinations of quantum numbers, using the minimum bias data.

The projection on $\Delta\phi_{\Lambda,\overline{p}}$, $\Delta\phi_{\Lambda,\overline{D}}$ of the opposite baryon opposite charm correlation function is shown in the upper left corner of Figure 9. We can see that the significance of the ridges in $\Delta\phi_{\Lambda,\overline{D}}$ and $\Delta\phi_{\Lambda,\overline{p}}$ have changed compared to the forced charm production. In the forced charm production, the $\Delta\phi_{\Lambda,\overline{D}} = \pi$ dominates, while the ridge around $\Delta\phi_{\Lambda,\overline{p}} = 0$ is much smaller. In the minimum bias, the latter dominates, with a smaller ridge around $\Delta\phi_{\Lambda,\overline{D}} = 0$. The balancing particles tend to be close to the triggering charmed baryon. There is also a slight diagonal ridge where $\Delta\phi_{\Lambda,\overline{p}} = \phi_{\Lambda,\overline{D}}$ and the balancing baryon follows the balancing charm.

The same projection is shown in the lower left corner of Figure 9 for the opposite baryon same charm correlation function. Removing the initial forced charm production does not significantly change the shape of this correlation function. The same charmed particles are produced similarly as in the forced charm production, with the balancing baryon being close to the trigger particle and the charmed meson disfavouring being close to the charmed baryon.

The upper right corner of Figure 9 shows the same baryon opposite charm correlation function. The bias of proximity between opposite charm particles seen in the opposite baryon opposite charm is also visible in the same baryon opposite charm correlation function. It is interesting to note that the same baryon number particles are mainly located back-to-back, as can be seen in the diffused peak on the away side.

Lastly, the same baryon same charm projection is shown in the lower right corner of Figure 9. The same baryon same charm in minimum bias is similar to the forced charm production since they are not as affected by removing the forced charm production. Par-

ticles with the same quantum number as the trigger are mainly back-to-back with it, disfavouring closeness.

4.2.2 Projection on $\Delta\eta_{\Lambda,p(\overline{p})}$ and $\Delta\eta_{\Lambda,D(\overline{D})}$

Figure 10 shows the correlation functions projected on $\Delta\eta_{\Lambda,p(\overline{p})}$, $\Delta\eta_{\Lambda,D(\overline{D})}$ for the minimum bias.

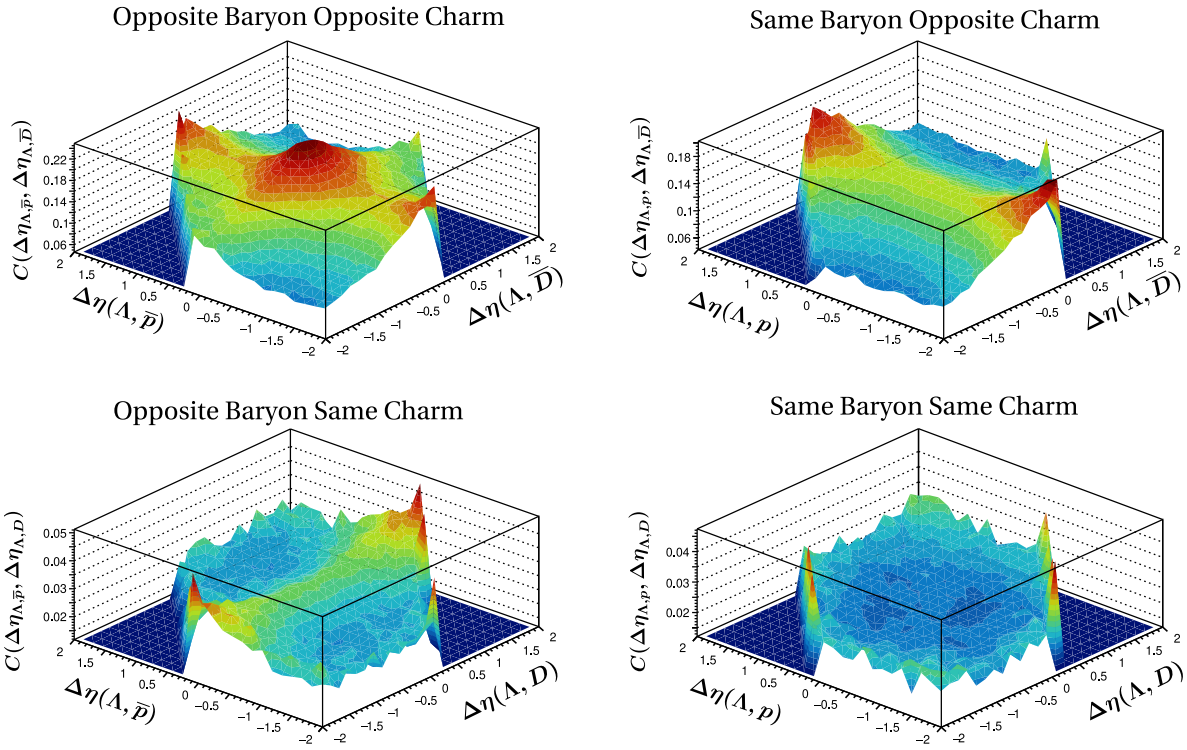

Figure 10: Correlation functions projected on $\Delta\eta_{\Lambda,p(\overline{p})}$, $\Delta\eta_{\Lambda,D(\overline{D})}$ for the different combinations of quantum numbers, using the minimum bias data.

Firstly, the opposite baryon opposite charm correlation function is shown in the upper left corner of Figure 10. Both the balancing charmed meson and the balancing light baryon are located close by the triggering charmed baryon, with a peak at $\Delta\eta_{\Lambda,\overline{p}} = \Delta\eta_{\Lambda,\overline{D}} = 0$.

The opposite baryon same charm projection is shown in the lower left corner of Figure 10. The ridge around $\Delta\eta_{\Lambda,\overline{p}} = 0$ clearly shows that the baryons are close to each other. The charmed baryon and meson, which in this triplet have the same charm number, are spread out with a slight disfavouring of proximity.

The upper right corner of Figure 10 shows the projection of the same baryon opposite charm correlation function. The opposite charmed particles in the triplet are close to each other in pseudorapidity, while the baryon with the same baryon as the trigger particle is spread out in pseudorapidity relative to the trigger. Again, we see a slight disfavouring of close proximity.

Lastly, the same baryon same charm correlation function is shown in the lower right

corner of Figure 10. There is again no clear correlation in pseudorapidity between the particles in the triplet with the same baryon number and same charm.

4.2.3 Discussion

We can see that in the minimum bias, the charmed particles with opposite quantum numbers are located close to each other both in azimuthal angle and pseudorapidity. This is in stark contrast to the forced charm production where the $c\bar{c}$ pair is produced back-to-back in azimuthal angle and spread out in pseudorapidity. This indicates that the $c\bar{c}$ pairs are more likely to be produced from a hard gluon with transverse momentum in the lab frame (see Figure 2, right) than in the initial hard scattering (see Figure 2, left). Another feature that is visible in the projections of the correlation functions on $\Delta\eta$ is that the signal for the opposite baryon opposite charm looks to partly be composed of the signals of the other correlation functions. This highlights again the importance of the balance function since only looking at the opposite baryon opposite charm three-particle correlation does not show the correlations that are purely between baryon and charm number production. In other words, the opposite baryon opposite charm correlation also includes particle triplets in which not all particles are produced on the same string in Pythia, so we cannot yet use this to understand the all production mechanisms at play.

4.3 Balance Function Forced Charm Production

Next, we present the balance function as defined in equation (14), projected on all four relevant combinations of axes as given by equation (10)-(13).

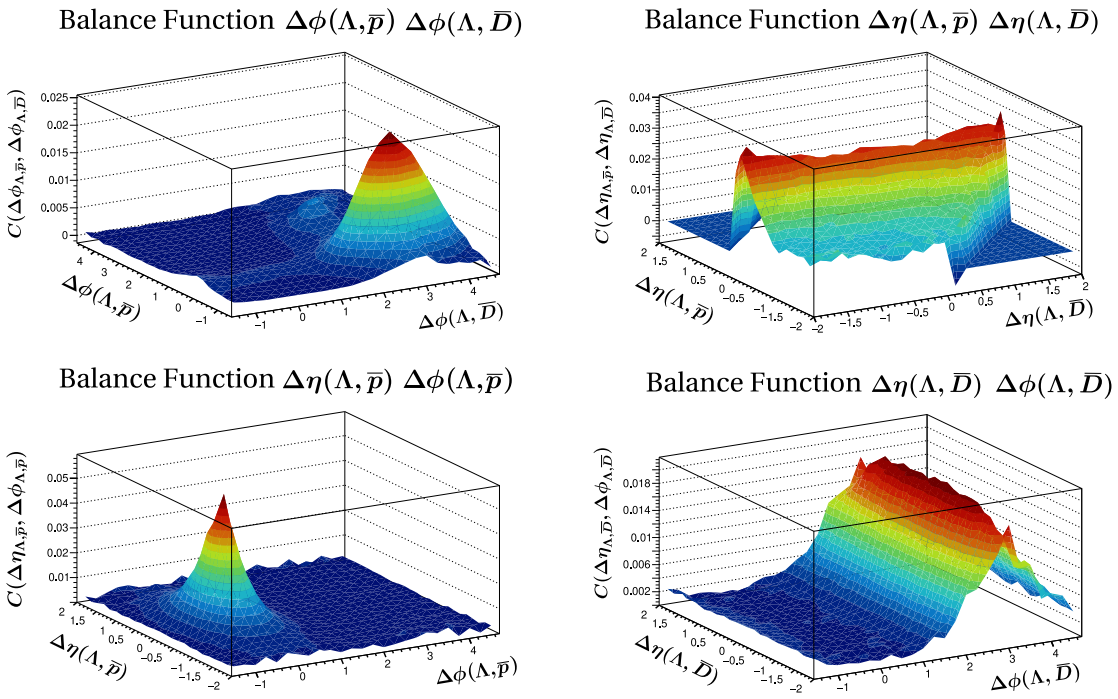

Figure 11: Projections of the balance function for baryon number and charm, $C(\Delta\phi_{\Lambda,\bar{p}}, \Delta\phi_{\Lambda,\overline{D}}, \Delta\eta_{\Lambda,\bar{p}}, \Delta\eta_{\Lambda,\overline{D}})$, for forced charm production, where Λ, $\bar{p}$ and $\overline{D}$ are defined as in Table 4.

In the balance function the random combinations of Λ, $\overline{p}$ and Λ, $\overline{D}$ are removed, by assuming that pairs from different interactions should behave equivalently to the uncorrelated pairs of Λ, p and Λ, D. Looking at the upper two plots, we can see that there is a real three-particle correlation between charmed baryons, light baryons and charmed mesons. If this would not be the case, the balance function would cancel out and be flat. The $\Delta\phi_{\Lambda,\overline{p}}$, $\Delta\phi_{\Lambda,\overline{D}}$ projection is similar to the opposite baryon number opposite charm presented prior, but is here corrected for uncorrelated, random pairs of particles. This enhances the significance of the peak at $(\Delta\phi_{\Lambda,\overline{p}}, \Delta\phi_{\Lambda,\overline{p}}) = (0, \pi)$, telling us that the balancing charmed particle is produced back-to-back to the pair of the triggering charmed baryon and the balancing baryon. The peak in $\Delta\phi_{\Lambda,\overline{D}}$ on the away side is a result of the forced charm production, as has been mentioned in earlier discussions. This is even more clear in the lower right corner, showing the projection of $\Delta\phi_{\Lambda,\overline{D}}$ and $\Delta\eta_{\Lambda,\overline{D}}$, which highlights the back-to-back correlation in azimuthal angle. Each event starts with a hard scattering producing a $c\overline{c}$ pair, which are back-to-back in ϕ but distributed in η for the total momentum to be conserved. In the projection of the balance function on pseudo-rapidity, we see that the balancing charmed meson is spread out in η, while the baryons have similar transverse momentum and are located close to each other in η. Note that if $\Delta\eta_{\Lambda,\overline{p}} \in [0, -2]$ then $\Delta\eta_{\Lambda,\overline{D}} \in [0, -2]$ as well (the same goes for the other side of the range), as a result of the acceptance range $|\eta| \leq 1$. The close proximity of the baryons is also visible in the lower left corner of Figure 11, showing the projection of the balance function on $\Delta\eta_{\Lambda,\overline{p}}$ and $\Delta\phi_{\Lambda,\overline{p}}$ where opposite baryon number particles are produced near in phase space.

These results can be understood by considering the production of particles in Pythia. Since the balance function has been corrected for uncorrelated, random particle pairs, it describes a scenario in which all three particles in the triplet are formed on the same string in Pythia, as was shown in Figure 4. In Pythia, the charm anti-charm quarks are placed on the ends of the strings, since they are only produced in hard processes. With initial hard scattering producing the $c\overline{c}$, these are back-to-back for momentum conservation reasons. The string breaks into quark antiquark and diquark pairs producing new particles. To produce the baryons of interest, the string has to break into two quark antiquark pairs of up and down quarks (and the corresponding antiparticles) so that the baryons travel together in momentum space. This is consistent with what is observed in the projections of the balance function. It should also be noted that the results have now been discussed as though all particles analysed are $\Lambda_c^+(\Lambda_c^-)$, $D^0(\overline{D^0})$ and $p(\overline{p})$. Similar arguments can be made for triplets made up of other particles. Furthermore, the analysis was also done selecting only $\Lambda_c^+(\Lambda_c^-)$, $D^0(\overline{D^0})$ and $p(\overline{p})$, giving the same results but with significantly smaller data sets.

To summarise the balance function: if forced charm production is in place, there is a correlation between baryon number and charm number production, namely the balancing charm being produced back-to-back in ϕ to the balancing baryon number, and evenly distributed in η. The particles with opposite baryon number are produced close together in momentum-space, while the particles with opposite charm quantum number are back-to-back in azimuthal angle and evenly distributed in $\Delta\eta$. This can be explained by considering the production mechanisms present in the string model used in Pythia to generate the particles.

4.4 Balance Function Minimum Bias

Next, we present the balance function for the minimum bias, where the condition on initial charm production is removed. The four projections of the balance function as defined in equation (10)-(13) are shown in Figure 12.

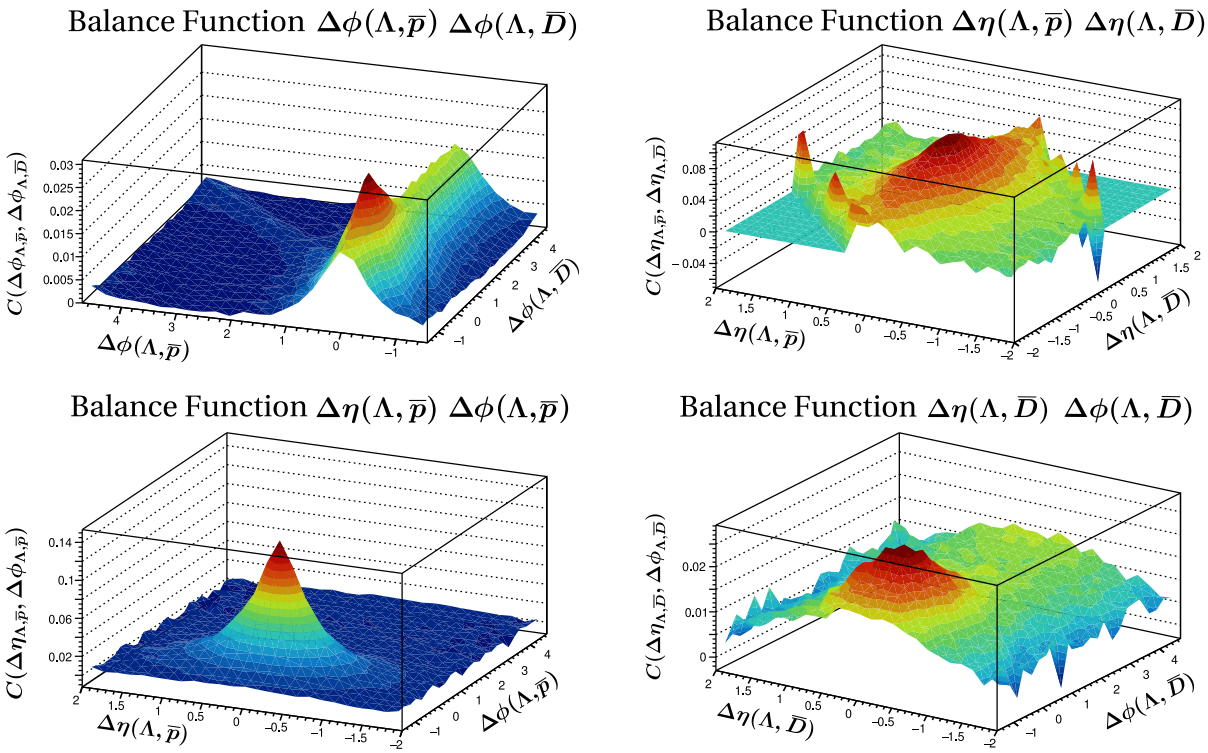

Figure 12: Projections of the balance function for baryon number and charm, $C(\Delta\phi_{\Lambda,\overline{p}}, \Delta\phi_{\Lambda,\overline{D}}, \Delta\eta_{\Lambda,\overline{p}}, \Delta\eta_{\Lambda,\overline{D}})$, for minimum bias, where Λ, $\overline{p}$ and $\overline{D}$ are defined as in Table 4.

We see that the shape of the projection on $\Delta\phi_{\Lambda,\overline{p}}$, $\Delta\eta_{\Lambda,\overline{p}}$ remains unchanged compared to the forced charm production, while the other three projections change significantly. The baryon balancing the trigger is produced close to it, both in pseudorapidity and azimuthal angle. Without the forced charm production, the balancing charmed hadron is also produced close to the trigger, mainly following the balancing baryon. This can be seen in the upper two plots, showing the projections on $\Delta\phi_{\Lambda,\overline{p}}$, $\Delta\phi_{\Lambda,\overline{D}}$ and $\Delta\eta_{\Lambda,\overline{p}}$, $\Delta\eta_{\Lambda,\overline{D}}$. The main peak in the projection on the azimuthal angle is located at $\Delta\phi_{\Lambda,\overline{p}} = \Delta\phi_{\Lambda,\overline{D}} = 0$, but there is a small ridge along the diagonal where the balancing charmed meson follows the balancing light baryon. There is still a slight spread in the distribution of the charmed hadrons, which is also visible in the projection of the balance function over the pseudorapidity. The peak is still located at $\Delta\eta_{\Lambda,\overline{p}} = \Delta\eta_{\Lambda,\overline{D}} = 0$. The baryons travel together with the charmed meson being close to them, if a bit more diffused in momentum space. This can also be seen in the lower right corner of Figure 12 showing the projection of the balance function on $\Delta\phi_{\Lambda,\overline{D}}$, $\Delta\eta_{\Lambda,\overline{D}}$. The base level of this projection is above zero, with a preference of $\Delta\phi_{\Lambda,\overline{D}} = \Delta\eta_{\Lambda,\overline{D}} = 0$, but it is interesting to note that the peak in the correlation function of the charmed hadrons is much more diffused than the baryons. This could mean that the charmed particles are produced before the baryons, giving them more time to spread out.

For the minimum bias, the hard initial correlation of $\Delta\phi_{\Lambda\overline{D}} = \pi$ is removed. In practice, this means that the charm pairs produced via pair-production of gluons become more significant than with the forced charm production in place. Since the hard gluons have a high transverse momentum in the lab frame, the quark pair can travel close together. However, since the charm quark is massive compared to the up, down and strange quark, it is heavily suppressed in the string breakings in Pythia and the $c\overline{c}$ will still be mainly located at the end of the strings. We would therefore expect some spread in $\Delta\phi_{\Lambda,\overline{D}}$, but with a localised peak at $\Delta\phi_{\Lambda,\overline{D}} = \Delta\eta_{\Lambda,\overline{D}} = 0$. The same arguments as for the light baryon production with forced charm production holds for the light baryons with minimum bias. This behaviour shows up as expected in the balance function. There is no excess signal around $\Delta\phi_{\Lambda,\overline{D}} = \pi$, showing that in a more realistic case most of the initial, head-on hard scatterings do not generally produce $c\overline{c}$ pairs.

To summarise, in the case of the minimum bias the dominating correlation is that the balancing baryon and balancing charmed particle both follow the triggering charmed baryon. There is also a slight tendency for the balancing charmed meson to be located anywhere in momentum space compared to the balancing baryon. In addition, there is a slight tendency for the balancing baryon and balancing charmed meson to follow each other independently of the triggering charmed baryon.

4.5 Ranges Forced Charm Production

Next, we present the results for another approach to investigate possible correlations of baryon and charm quantum number, namely the ranges. These are obtained by requiring the light and charmed baryon pair to be produced somewhere in phase space and investigating what this does to the charmed meson. The set range correlation is compared to the no set range correlation by means of dividing the set range correlation projected on $\Delta\phi_{\Lambda,D(\overline{D})}$ and $\Delta\eta_{\Lambda,p(\overline{p})}$ with the original, no set range. This fraction is in turn projected on $\Delta\phi_{\Lambda,D(\overline{D})}$, giving

$$\frac{C'(\Delta\phi_{\Lambda,D(\overline{D})}\ )}{C(\Delta\phi_{\Lambda,D(\overline{D})}\ )} = \left(\frac{1}{N^{(x)}_{\Lambda,p(\overline{p})}}\frac{dN'}{d\Delta\phi_{\Lambda,D(\overline{D})}}\right) \Big/ \left(\frac{1}{N_{\Lambda,p(\overline{p})}}\frac{dN}{d\Delta\phi_{\Lambda,D(\overline{D})}}\right). \tag{17}$$

The fractions are shown in Figure 13 for the four ranges listed in section 3.4. The correlation functions with set range, before and after taking the fraction, are shown in the Appendix.

It should be noted that because the triggering method is different for these correlation functions than for the correlation functions used to produce the balance function, it is not possible to quantitatively compare the two. We will therefore qualitatively discuss the graphs rather than focus on the numerical values given by the fraction. The fraction in essence tells you how large the probability is to find the charmed pair at a certain $\Delta\phi$ when the pair of baryons is fixed in a range of $\Delta\phi$, with respect to the probability it has to be found there when the baryon pair is not fixed. If the location of the light baryon would not influence the charmed mesons, these fractions would all be flat at a certain value. This observable is something which was worked out from scratch in this project and a lot of trial and error was involved with regards to triggering, visualisation and interpretation. Further development of this observable would possibly give more clear results.

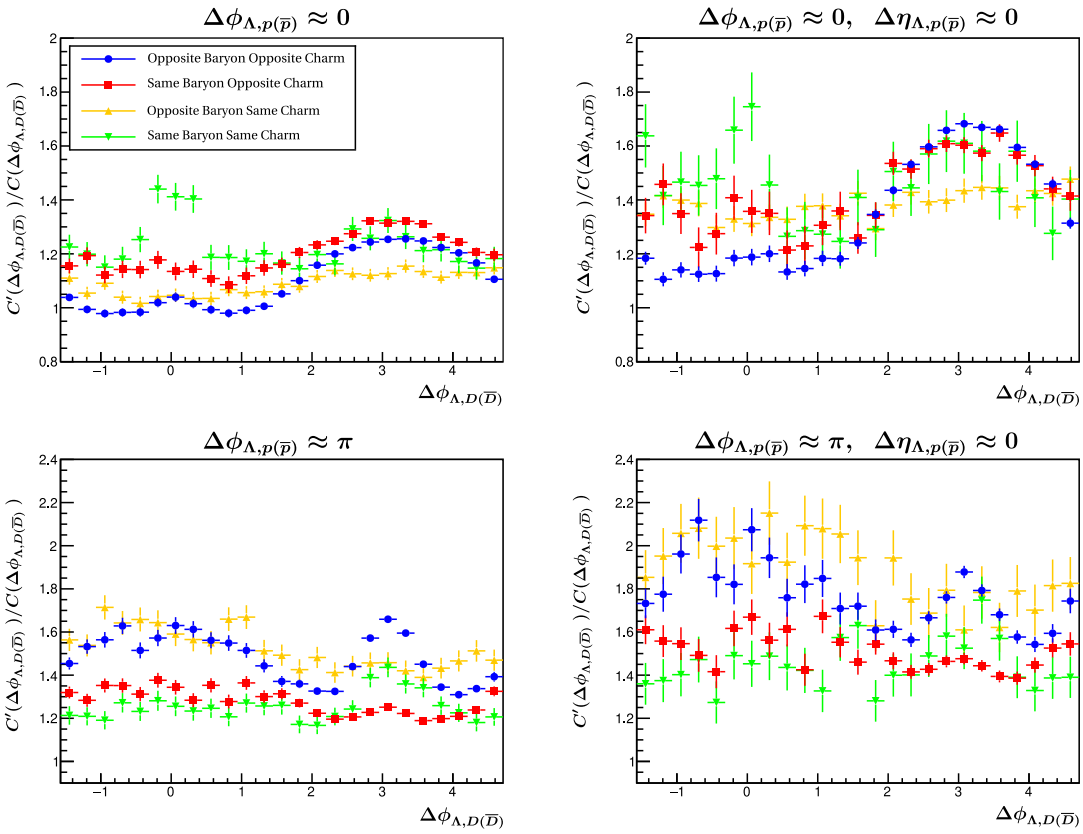

Figure 13: The fraction of the correlation functions with a set range on $\Delta\phi_{\Lambda,p(\overline{p})}$ and $\Delta\eta_{\Lambda,p(\overline{p})}$ with the original correlation function, for forced charm production. The fraction is projected on $\Delta\phi_{\Lambda,D(\overline{D})}$.

We start with looking at the opposite charm opposite baryon correlation. When the pair of baryons is required to be close to each other in phase space, as in the upper two graphs of Figure 13, the charmed pair of particles tends to be back-to-back. This is of no surprise and confirms what we have seen in previous correlations. In the initial hard process where the charm anti-charm pair is generated, the quarks are back-to-back. When the string tension increases and eventually breaks forming a diquark pair, producing the charmed baryon and light baryon, these tend to follow each other. Interestingly enough, there is also a small signal around $\Delta\phi_{\Lambda,\overline{D}} = 0$, where the charmed meson follows the baryons. Comparing the upper two graphs to the two lower graphs in Figure 13 in which the baryon pair is forced to be back-to-back, we see that there is a much more narrow peak on the away side for $\Delta\phi_{\Lambda,\overline{D}}$. When the charmed baryon and the light baryon are required to be back-to-back, the light baryon follows the charmed meson. The string breaking producing the $u\overline{u}$ quark pair shared by the charmed meson and light baryon becomes more significant than the diquark breaking. We still have a broad peak where the balancing charm is back-to-back to the balancing baryon and thereby close to the trigger particle.

The same baryon, opposite charm data show a similar preference for the opposite charm to be produced to the away side when the baryons are close together. What is interesting is that if the baryons are produced back-to-back, the peak at $\Delta\phi_{\Lambda,\overline{D}} = \pi$ is much smaller than for the opposite baryon, opposite charm. This is most likely because the uu quarks of the baryon and charmed meson are not shared by the same string. The same

baryon same charm shows that the charmed meson follows the light baryon. Because the charmed hadrons have the same charm quantum number they are either produced on different strings or through an additional, unlikely string-breaking producing charm anti-charm pairs. In essence, these are "random" pairs of particles. The opposite baryon same charm correlation shows no preference. These two correlations are also the datasets with the largest uncertainties. The reason for this is that this configuration would require two $c\bar{c}$ pairs to be produced within the same event, which is highly unlikely to happen.

4.6 Ranges Minimum Bias

Lastly, Figure 14 shows the fractions of the correlation functions with applied range and the correlation functions with no applied range, using the minimum bias data.

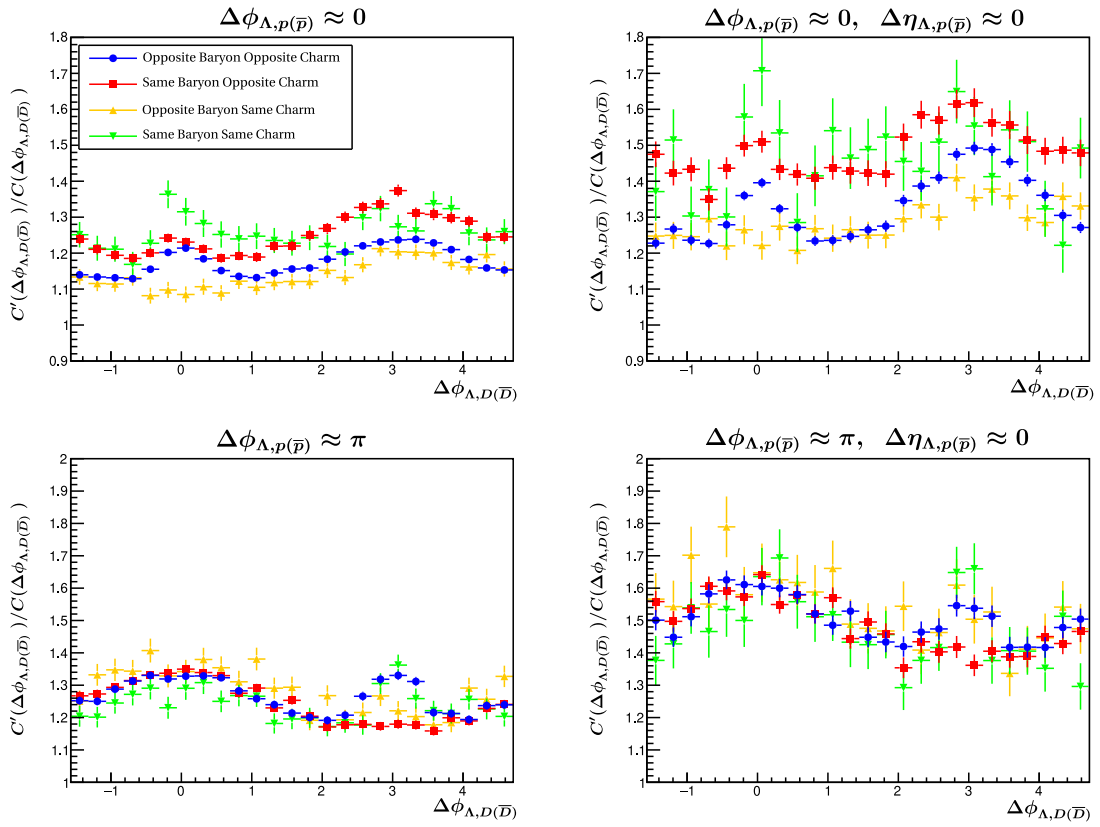

Figure 14: The fraction of the correlation functions with a set range on $\Delta\phi_{\Lambda,p(\overline{p})}$ and $\Delta\eta_{\Lambda,p(\overline{p})}$ with the original correlation function, for minimum bias. The fraction is projected on $\Delta\eta_{\Lambda,D(\overline{D})}$.

The changes of the ranges when going from forced charm production to minimum bias are again caused by the increase of the significance of the gluon pair-producing quark pairs, removing the prominent correlation at $\Delta\phi_{\Lambda,\overline{D}} = \pi$. As a result of this, opposite baryon opposite charm has a slightly more significant peak at $\Delta\phi_{\Lambda,\overline{D}} = 0$ when $\Delta\phi_{\Lambda,\overline{p}} = 0$. We have more charmed hadrons being close together than in the forced charm production. The charmed meson seems to follow the light baryon given by the peak around $\Delta\phi_{\Lambda,\overline{D}} = \pi$ when $\Delta\phi_{\Lambda,\overline{p}} = \pi$. There is still a low, broad peak where the charmed meson is produced back-to-back to the baryons. This could be a result of initial hard scattering processes and is a behaviour that is not as clearly visible in the balance function. When the baryons are

forced to be back-to-back in azimuthal angle, the charmed meson follows. Similarly to the forced charm production, the same baryon opposite charm correlation behaves similarly to the opposite baryon opposite charm when $\Delta\phi_{\Lambda,p} = 0$ but not when $\Delta\phi_{\Lambda,p} = \pi$, highlighting the fact that the correlation is between balancing charm and baryon. If the light baryon in the triplet is not balancing the trigger, the charm does not seem to follow it. It seems like the meson in the same baryon same charm correlation follows the baryon, while the opposite baryon same charm is relatively constant. However, the opposite baryon same charm and same baryon same charm have the smallest data sets, indicating again that it is unlikely to produce triplets which do not balance the quantum numbers.

5 Conclusion and Outlook

The aim of this thesis was to investigate the possible correlation between the production of baryon number and charm quantum number. This was done through the means of three-particle correlations, in which the relative momentum-space coordinates $\Delta\phi$ and $\Delta\eta$ were calculated between the triggering charmed baryon and the associated charmed meson and light baryon, for different combinations of quantum numbers. The data used in the analysis was simulated using the event generator Pythia8. Three-particle correlations are not used as widely as their two-particle counterparts, so challenges such as triggering, normalisation, visualisation and interpretation had to be tackled.

The three-particle correlations showed that the opposite baryon number particles show a strong correlation through near side peaks, where the trigger and the associated particle are produced close to each other in phase space. In the case of the same baryon number particles, there seems to rather be an anti-correlation on the near side, where the production of other baryons with the same baryon number is disfavoured near the trigger particle. A similar behaviour exists in the same charm correlations. For the opposite charm correlations, the forced charm production and minimum bias show two very different pictures. In the case of the forced charm production, there is a clear ridge around π in relative azimuthal angle, evenly distributed in pseudorapidity. In the minimum bias, there is instead a preference for closeness, both in pseudorapidity and azimuthal angle, with a peak on the near side.

In the collision, all quantum numbers need to be conserved, so any excess of the involved quantum numbers needs to be balanced by opposite quantum numbers. As a result, particle pairs with the same quantum number are likely to be from different interactions, i.e. different strings. The behaviour seen in these correlations is rather a consequence of overall momentum conservation in the underlying event than correlations between individual particles produced. To investigate the true correlation between balancing charm and baryon number and answer the research question, the balance function is constructed. This balance function shows clear signals, indicating that the production of these particle triplets and their quantum numbers is not random in momentum space. The balance function shows that in the case of forced charm production, the balancing charm is produced back-to-back to the balancing baryon. The balancing baryon follows the triggering charmed baryon in momentum space. For the minimum bias, the balancing charm mainly follows the balancing baryon, which in turn follows the triggering charmed baryon. In other words, the triplet seems to travel together through momentum space. The charmed meson is, with respect to the triggering charmed baryon, more diffused in

momentum space compared to the light baryon.

Another way the question posed in this thesis was answered was to require the baryon pair to be located in a certain $\Delta\phi_{\Lambda,p(\overline{p})}$ interval and see what that does to the $\Delta\phi_{\Lambda,D(\overline{D})}$. These ranges tell a similar story as the balance function. In the minimum bias, the balancing charm follows the balancing baryon. This is also, to a much smaller extent, visible in the charm production. The charm production is still dominated by the forced $c\bar{c}$ pair back-to-back. As has been mentioned these ranges are not, as of yet, fully finished observables. Further development of this method is highly recommended.

As has been discussed, the results presented can be understood through the lens of the string model for particle production in Pythia. Since the charm quarks are heavy, they are located on the ends of strings. In the case of the forced charm production, each event starts with a hard scattering producing a $c\bar{c}$ pair back-to-back. The string between them breaks into quark and di-quark pairs producing the balancing light baryon, which shares a diquark pair with the charmed baryon and is therefore close to it, and the charmed meson. In the case of the minimum bias not every event starts with the $c\bar{c}$ pair being back-to-back, and so the $c\bar{c}$ pair produced via gluon pair-production, which is close together in phase space, becomes more significant.

One obvious future step is to compare the results presented to experimental data, once available. Other correlation studies, focusing on strange particles, found that strangeness and baryon number conservation are more localised in Pythia than in experimental data [17]. It would be interesting to see if that also applies to charmed particles. It should be noted that for comparing to experimental data the minimum bias results should be considered. In the wait for the higher energies and multiplicities at LHC and other particle accelerators needed to produce enough statistics with charmed hadrons, there are further steps that could be taken within the constraints of simulated data. The current set of data is either forced charm production or minimum bias. In the forced charm production, the correlations are dominated by the hard scattering correlation of $\Delta\phi_{\Lambda,\overline{D}} = \pi$, while the minimum bias includes many production mechanisms. It might be interesting to make these correlation functions depend also on the transverse momentum, to probe the production at different energy scales throughout the collision. It would also be interesting to apply the same analysis on simulated data using other extensions of Pythia, such as the so called junctions, or even completely different event generators. Another approach would be to increase the multiplicity of the events used in the analysis and approach larger system collisions, to see if the production mechanisms for charm and baryon number observed in these proton-proton collisions are different in large collision systems. Probing the production of quantum numbers in large systems might also give insight into the thermalisation and hadronisation of the QGP.

6 References

[1] C. Bierlich et al. "A comprehensive guide to the physics and usage of PYTHIA 8.3". In: *arXiv* (Mar. 2022). DOI: 10.48550/arXiv.2203.11601. eprint: 2203.11601.

[2] ALICE Collaboration. "The ALICE experiment at the CERN LHC". In: *J. Instrum.* 3.08 (Aug. 2008), S08002. ISSN: 1748-0221. DOI: 10.1088/1748-0221/3/08/S08002.

[3] *Standard Model of Elementary Particles*. [Online; accessed 6. Apr. 2023]. Apr. 2023. URL: https://upload.wikimedia.org/wikipedia/commons/0/00/Standard_Model_of_Elementary_Particles.svg.

[4] B. R. Martin and G. Shaw. *Particle physics /*. Fourth edition. The Manchester physics series. Chichester, West Sussex, United Kingdom : John Wiley Sons, Ltd., 2017.

[5] L. Garren et al. "Monte carlo particle numbering scheme". In: *Eur. Phys. J. C* 15.1 (Mar. 2000), pp. 205–207. ISSN: 1434-6052. DOI: 10.1007/BF02683426.

[6] *Charmed Baryons*. [Online; accessed 13. Apr. 2023]. 2006. URL: https://pdg.lbl.gov/2007/tables/bxxxcharm.pdf.

[7] *p*. [Online; accessed 13. Apr. 2023]. 2022. URL: https://pdg.lbl.gov/2022/listings/rpp2022-list-p.pdf.

[8] *n*. [Online; accessed 13. Apr. 2023]. 2022. URL: https://pdg.lbl.gov/2022/listings/rpp2022-list-n.pdf.

[9] $D^{\pm}$. [Online; accessed 13. Apr. 2023]. 2022. URL: https://pdg.lbl.gov/2022/listings/rpp2022-list-D-plus-minus.pdf.

[10] D^{0}. [Online; accessed 13. Apr. 2023]. 2022. URL: https://pdg.lbl.gov/2022/listings/rpp2022-list-D-zero.pdf.

[11] W. Busza et al. "Heavy Ion Collisions: The Big Picture, and the Big Questions". In: *arXiv* (Oct. 2018). DOI: 10.1146/annurev-nucl-101917-020852. eprint: 1802.04801.

[12] ALICE Collaboration. "Enhanced production of multi-strange hadrons in high-multiplicity proton-proton collisions". In: *arXiv* (Apr. 2017). DOI: 10.1038/nphys4111. eprint: 1606.07424.

[13] CMS Collaboration. "Observation of Long-Range Near-Side Angular Correlations in Proton-Proton Collisions at the LHC". In: *arXiv* (Sept. 2010). DOI: 10.1007/JHEP09(2010)091. eprint: 1009.4122.

[14] J. L. Nagle and W. A. Zajc. "Small System Collectivity in Relativistic Hadron and Nuclear Collisions". In: *arXiv* (Oct. 2018). DOI: 10.1146/annurev-nucl-101916-123209. eprint: 1801.03477.

[15] ALICE Collaboration. "Λ_c^+ production in pp collisions at $\sqrt{s} = 7$ TeV and in p-Pb collisions at $\sqrt{s_{\mathrm{NN}}} = 5.02$ TeV". In: *arXiv* (Apr. 2018). DOI: 10.1007/JHEP04(2018)108. eprint: 1712.09581.

[16] S. Acharya et al. "Measurement of D^0, D^+, D^{*+} and D_s^+ production in pp collisions at with ALICE". In: *Eur. Phys. J. C* 79.5 (May 2019). ISSN: 1434-6052. DOI: 10.1140/epjc/s10052-019-6873-6.

[17] J. Adolfsson. "Study of Ξ-Hadron Correlations in pp Collisions at $\sqrt{s}$ = 13 TeV Using the ALICE Detector". Available at https://portal.research.lu.se/en/publications/study-of-%CE%BE-hadron-correlations-in-pp-collisions-at-isi-13-tev-usi. PhD Thesis. Lund University, 2020.

[18] S. Basu et al. "Probing the Gluon Plasma with Charm Balance Functions". In: *arXiv* (Oct. 2021). DOI: 10.1140/epjc/s10052-021-09808-z. eprint: 2110.05134.

[19] R. Brun and F. Rademakers. *ROOT — An object oriented data analysis framework.* Version 6.26/10. DOI: https://root.cern/.

7 Appendix

7.1 Forced Charm Production

7.1.1 Correlation Functions

Below, the correlation functions for all four combinations of quantum numbers are shown projected over all four axes.

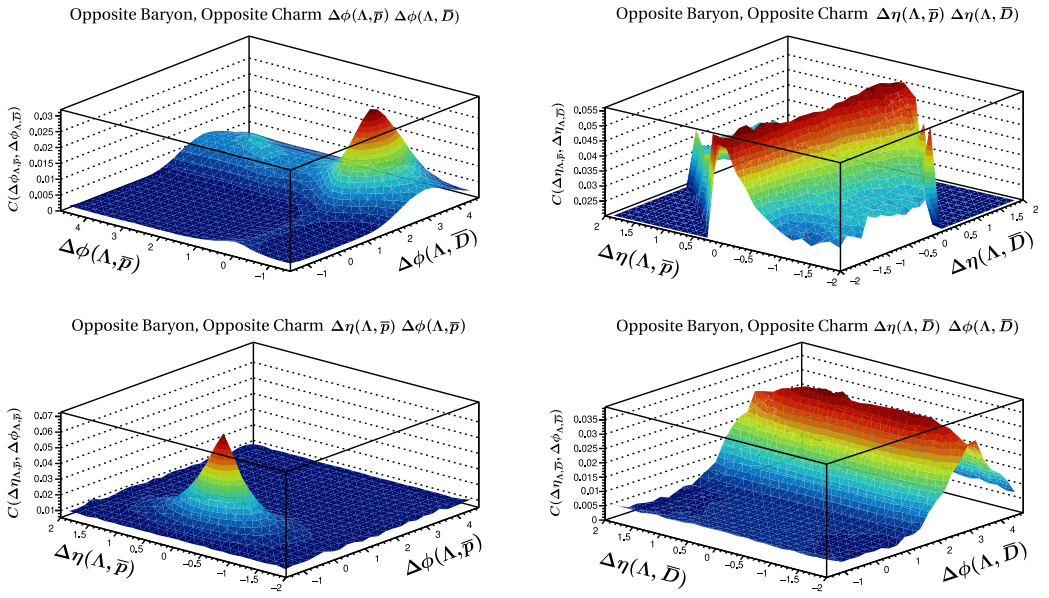

Figure 15: Projections of the correlation function for opposite baryon opposite charm, forced charm production.

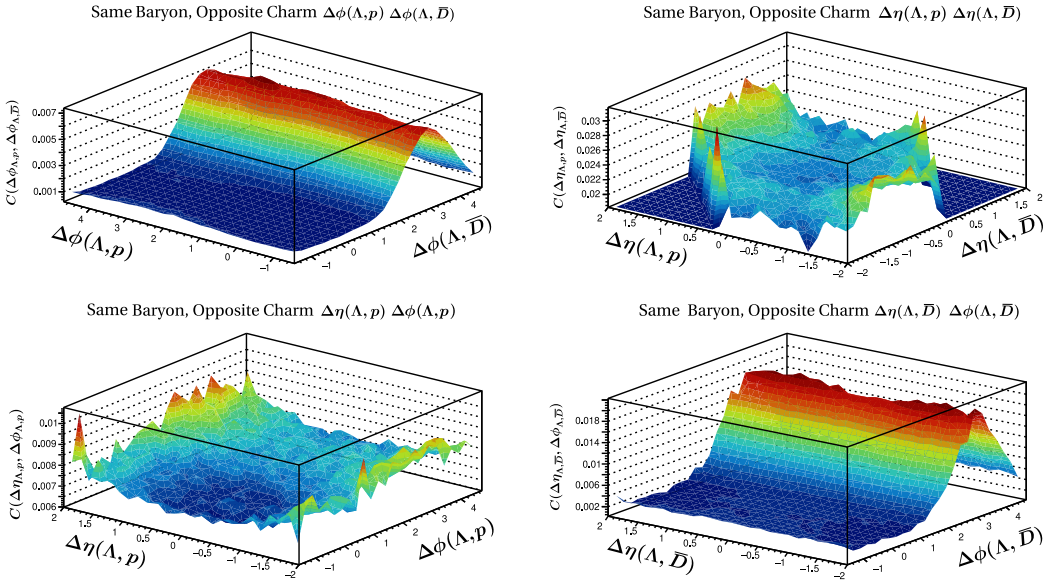

Figure 16: Projections of the correlation function for same baryon opposite charm, forced charm production.

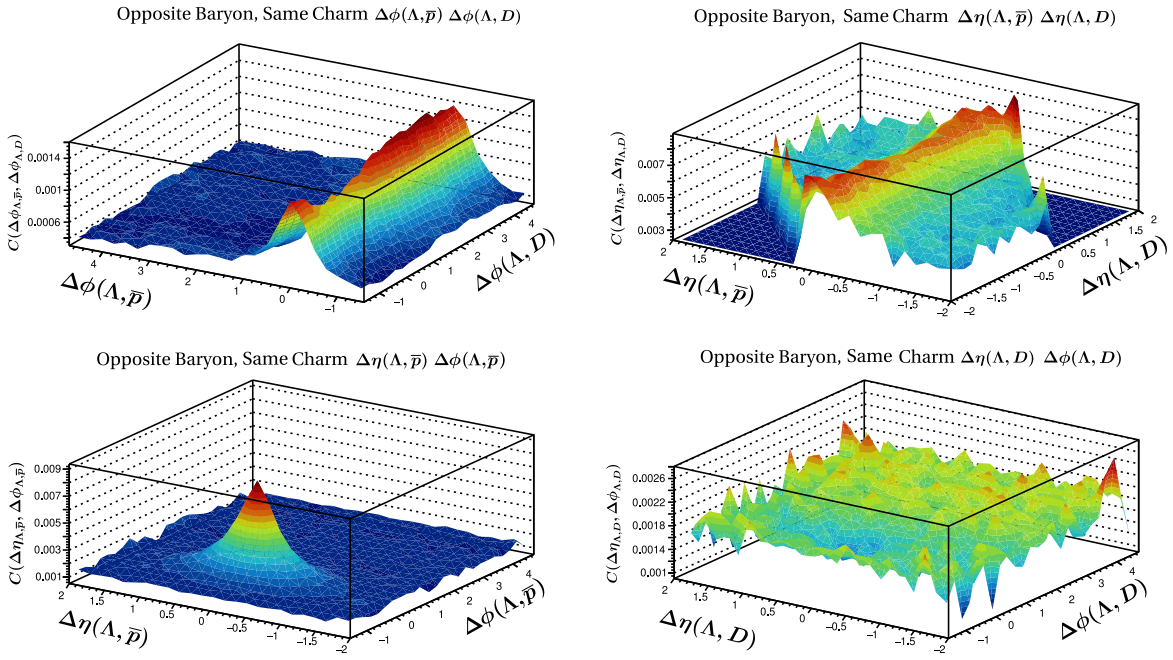

Figure 17: Projections of the correlation function for opposite baryon same charm, forced charm production.

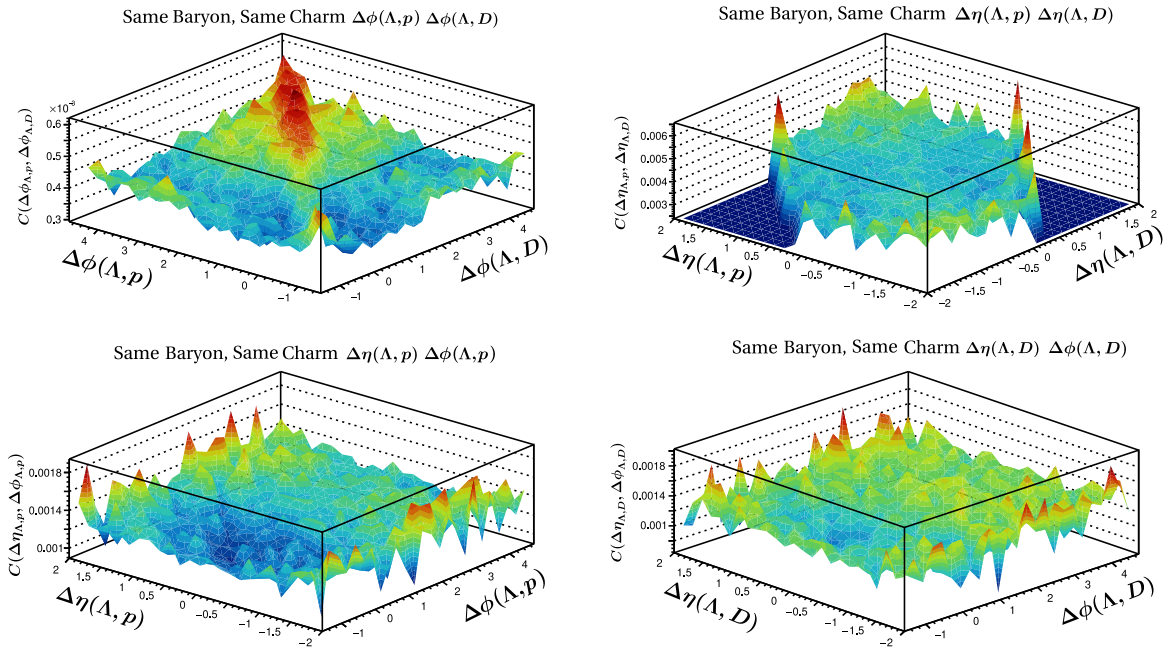

Figure 18: Projections of the correlation function for same baryon same charm, forced charm production.

7.1.2 Ranges Before Division

Below, the projections of correlation functions on $\Delta\phi_{\Lambda,D(\overline{D})}$, $\Delta\eta_{\Lambda,D(\overline{D})}$ for all four combinations are shown when $\Delta\phi_{\Lambda,p(\overline{p})}$ and $\Delta\eta_{\Lambda,p(\overline{p})}$ are fixed in the ranges (1)-(4). The order is as follows: upper right corner shows range (1), upper left corner shows range (2), lower right corner shows range shows range (3) and lower left corner shows range (4).

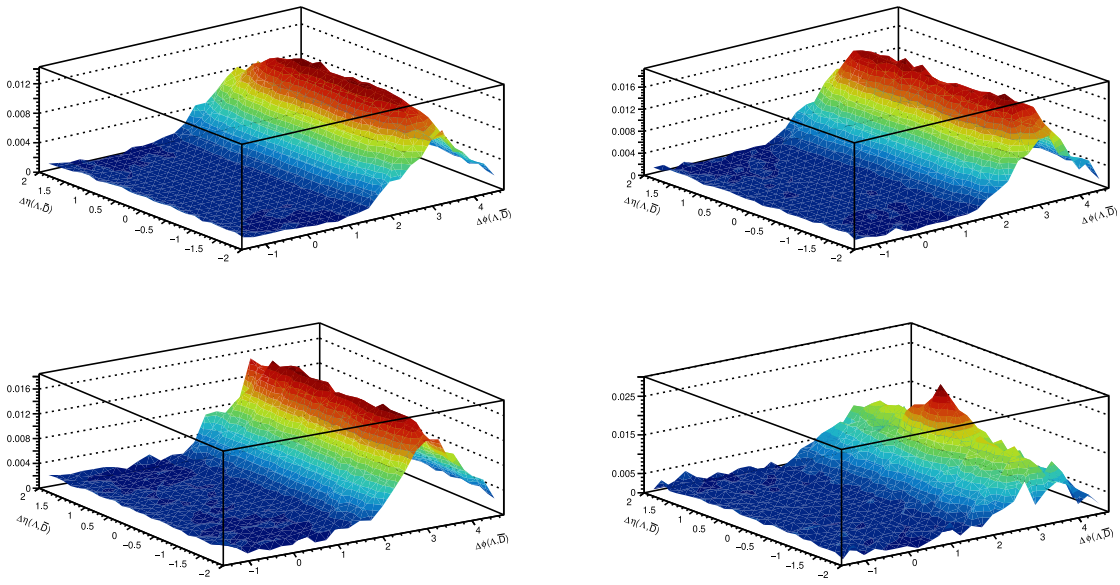

Figure 19: Opposite baryon opposite charm with applied ranges.

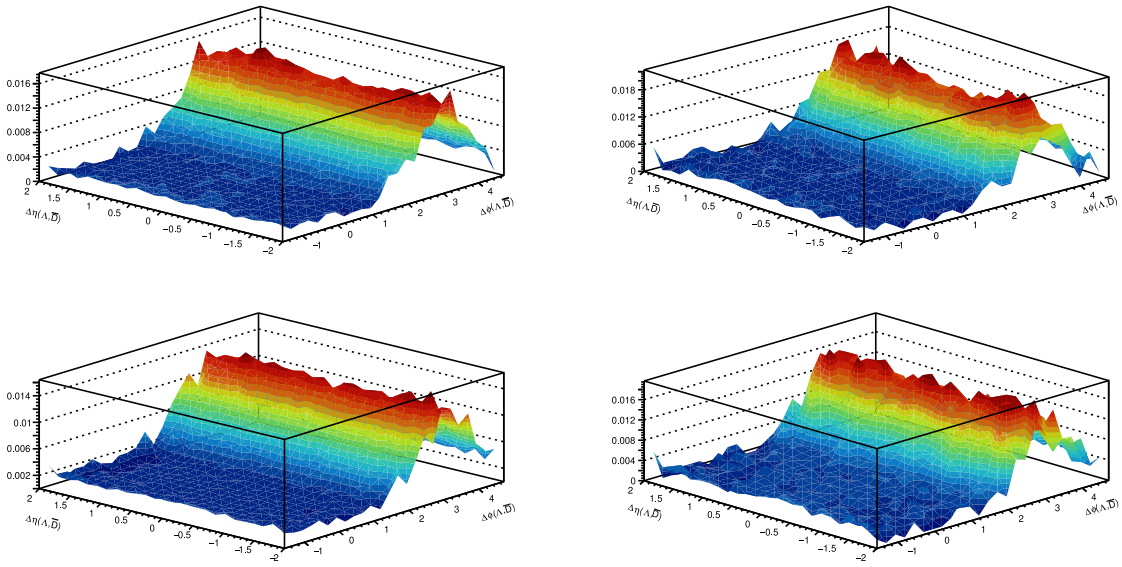

Figure 20: Same baryon opposite charm with applied ranges.

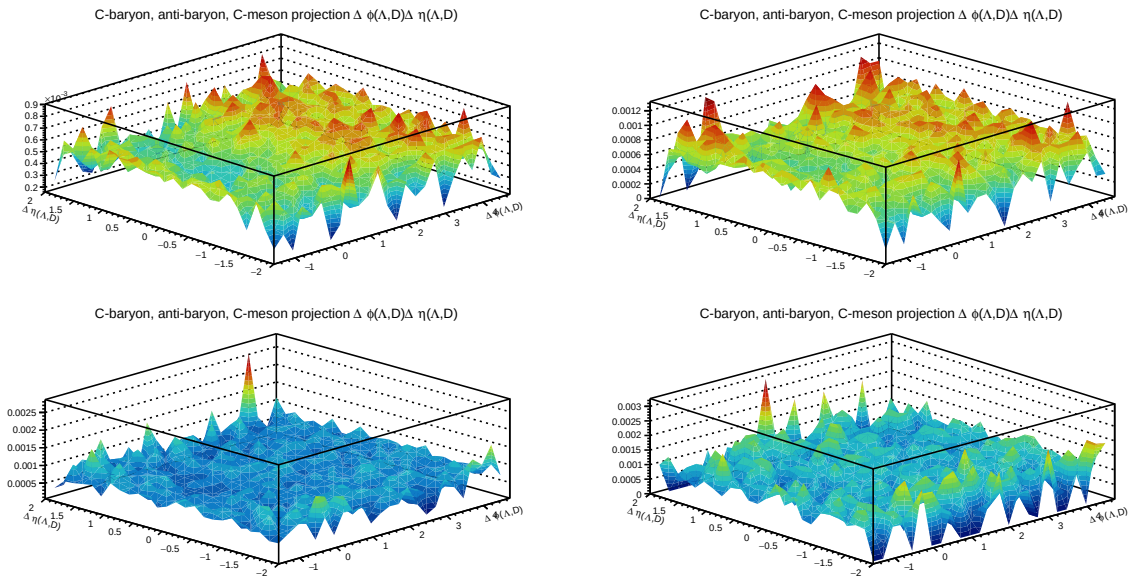

Figure 21: Opposite baryon same charm with applied ranges.

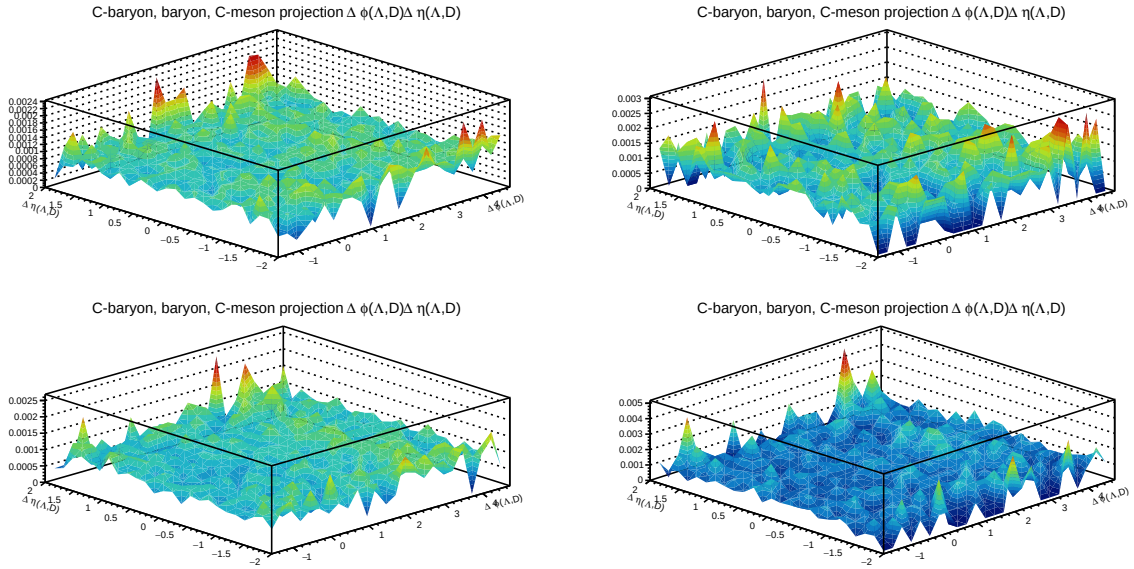

Figure 22: Same baryon same charm with applied ranges.

7.1.3 Ranges After Division

Below, the projections on $\Delta\phi_{\Lambda,D(\overline{D})}$ are shown for the fraction of the correlation function with set range over the correlation function without set range. The order is the same as in 7.1.2.

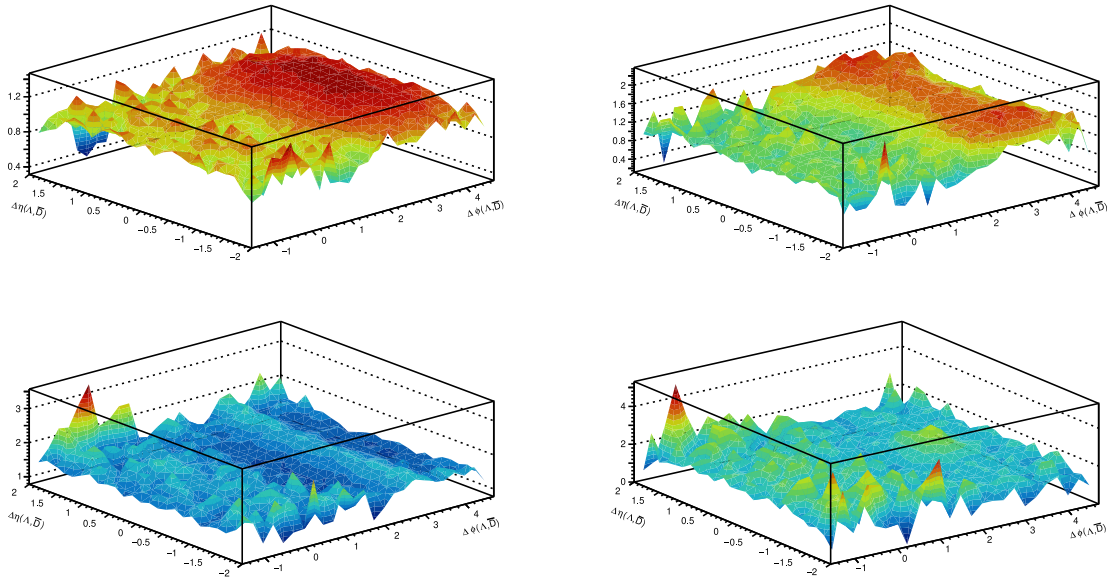

Figure 23: Fraction of range and no set range, opposite baryon opposite charm.

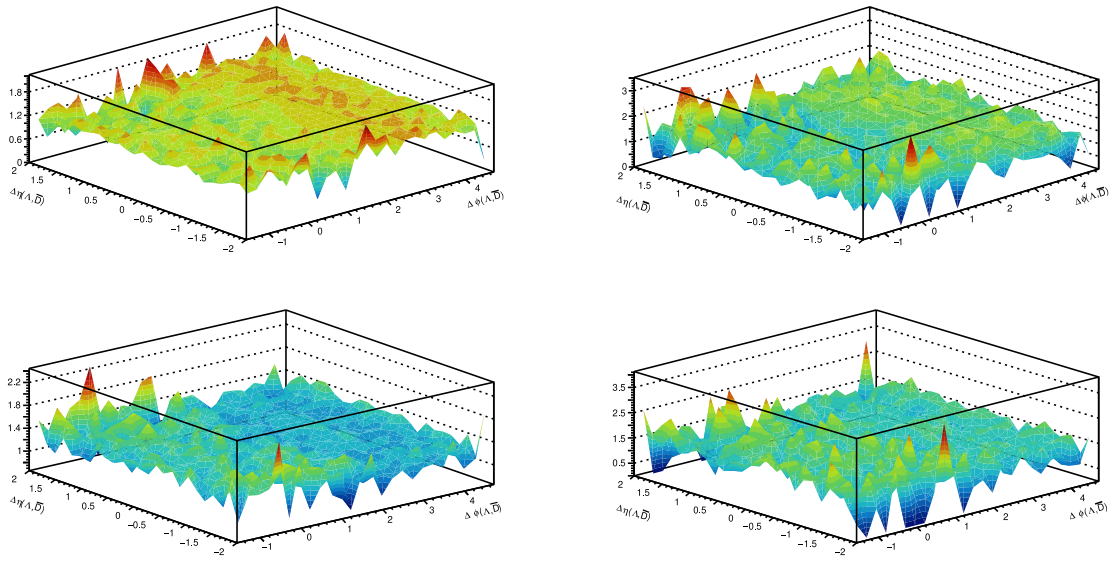

Figure 24: Fraction of range and no set range, same baryon opposite charm.

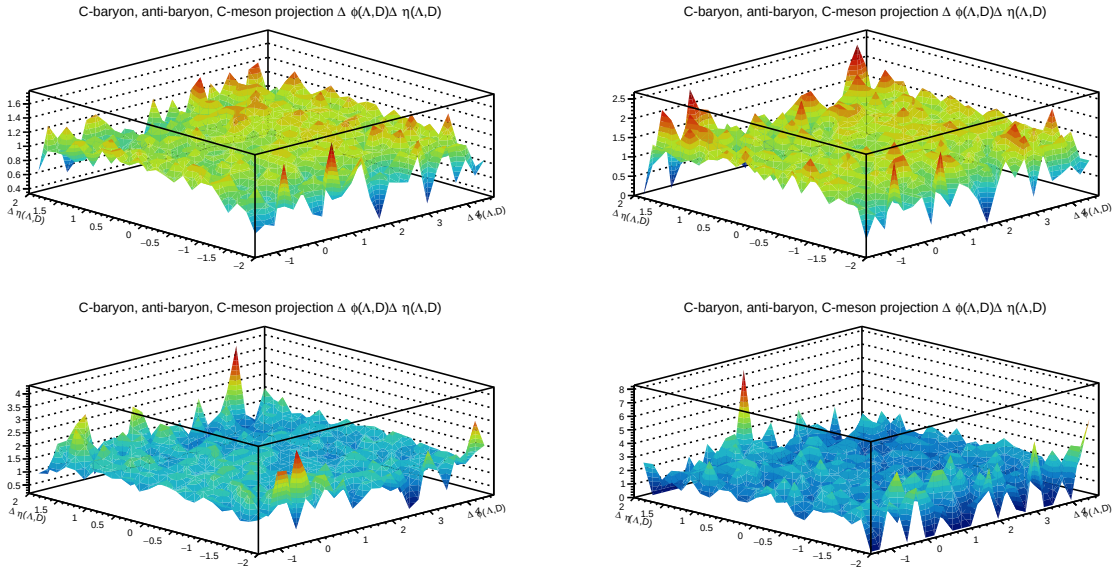

Figure 25: Fraction of the range and no set range, opposite baryon same charm.

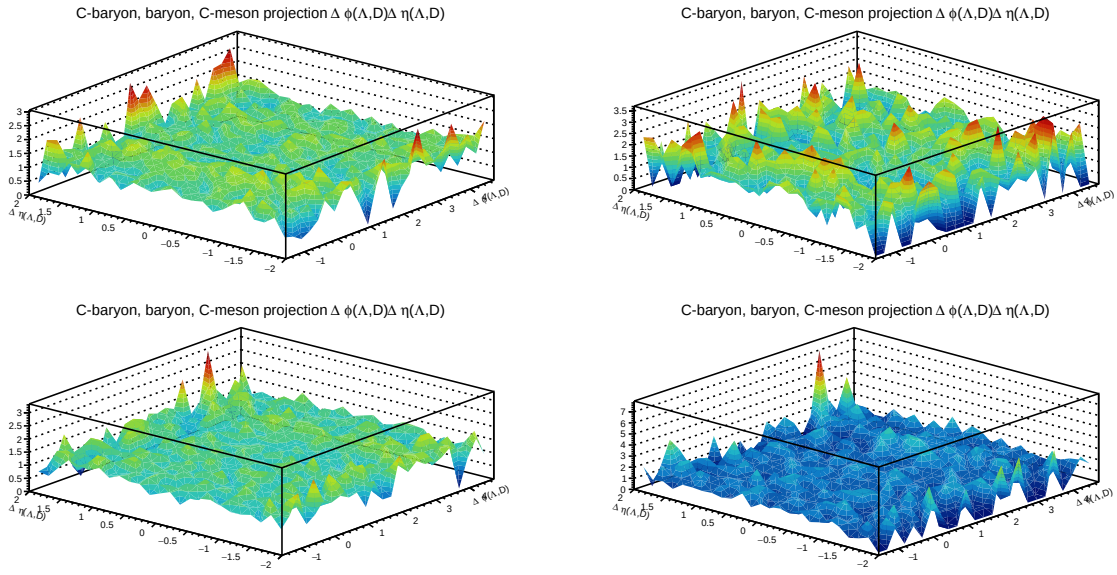

Figure 26: Fraction of the range and no set range, same baryon same charm.

7.2 Minimum Bias

7.2.1 Correlation Functions

Below, the correlation functions for all four combinations of quantum numbers are shown projected over all four axes.

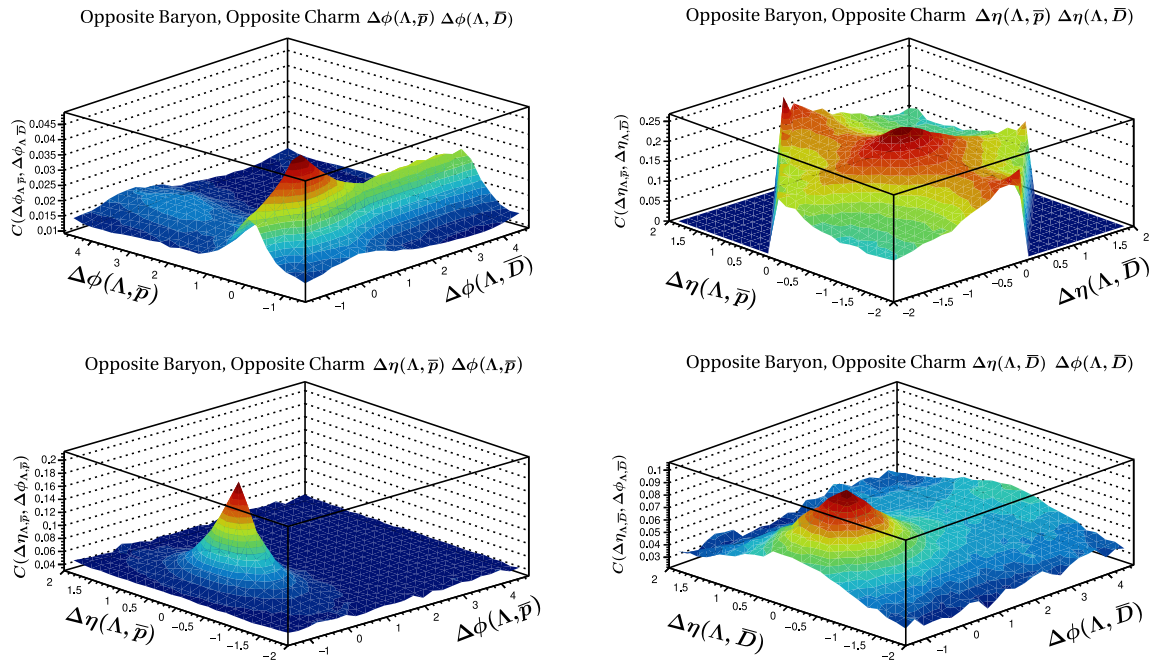

Figure 27: Projections of the correlation function for opposite baryon opposite charm, minimum bias.

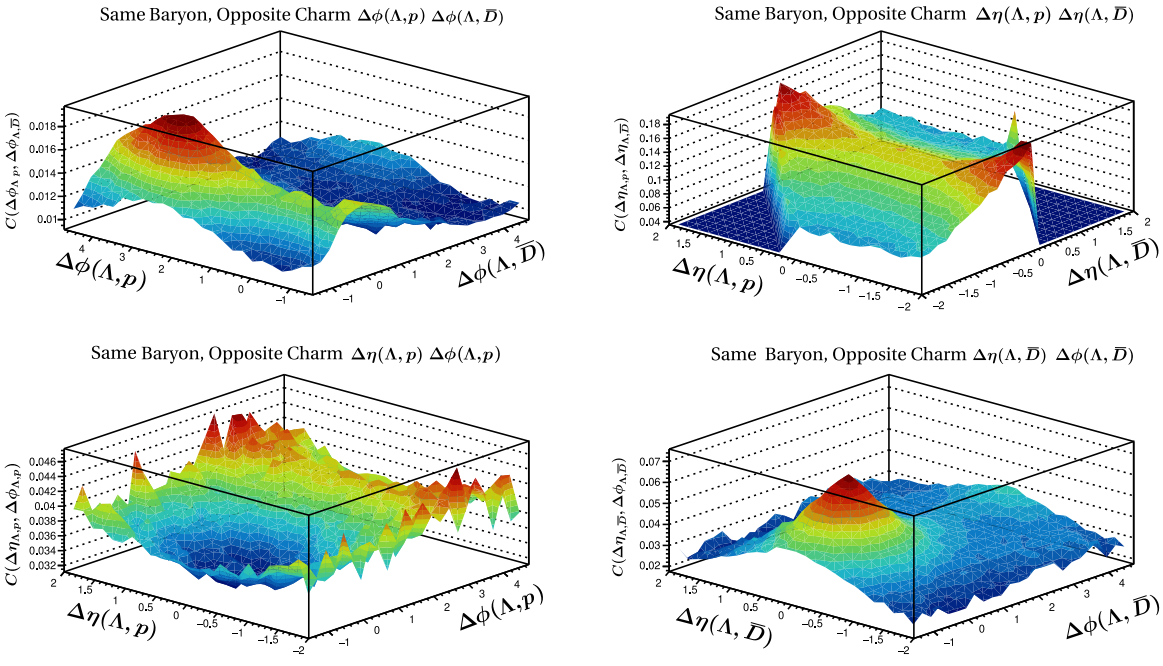

Figure 28: Projections of the correlation function for same baryon opposite charm, minimum bias.

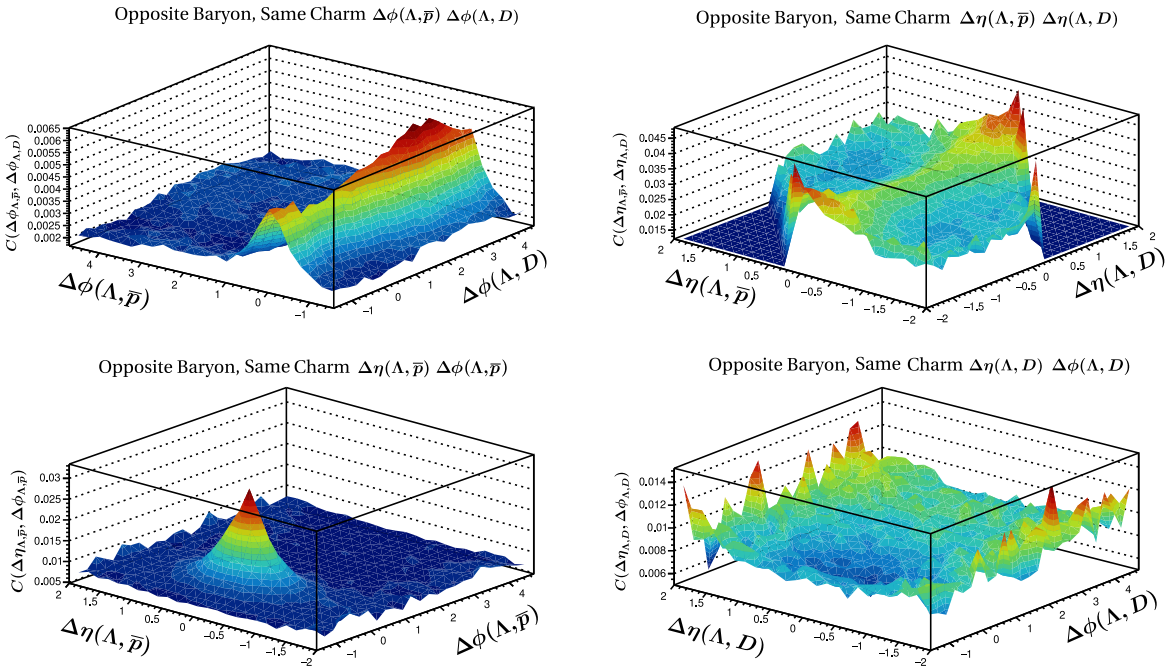

Figure 29: Projections of the correlation function for opposite baryon same charm, minimum bias.

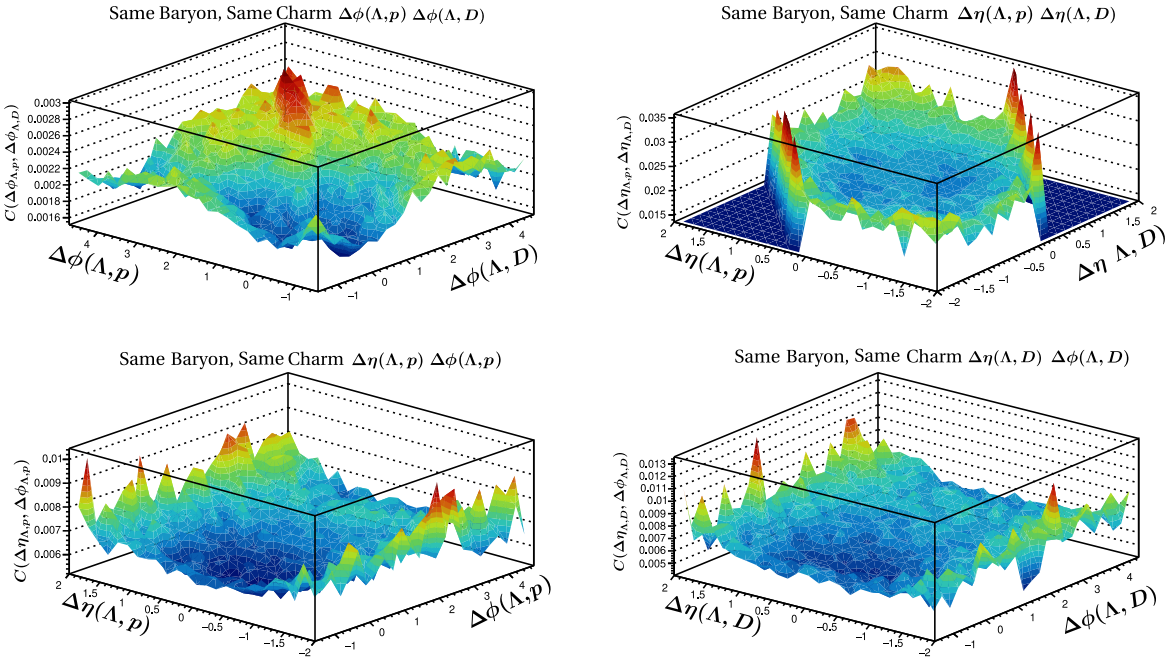

Figure 30: Projections of the correlation function for same baryon same charm, minimum bias.

7.2.2 Ranges Before Division

Below, the projections of correlation functions on $\Delta\phi_{\Lambda,D(\overline{D})}$, $\Delta\eta_{\Lambda,D(\overline{D})}$ for all four combinations are shown when $\Delta\phi_{\Lambda,p(\overline{p})}$ and $\Delta\eta_{\Lambda,p(\overline{p})}$ are fixed in the ranges (1)-(4). The order is as follows: upper right corner shows range (1), upper left corner shows range (2), lower right corner shows range shows range (3) and lower left corner shows range (4).

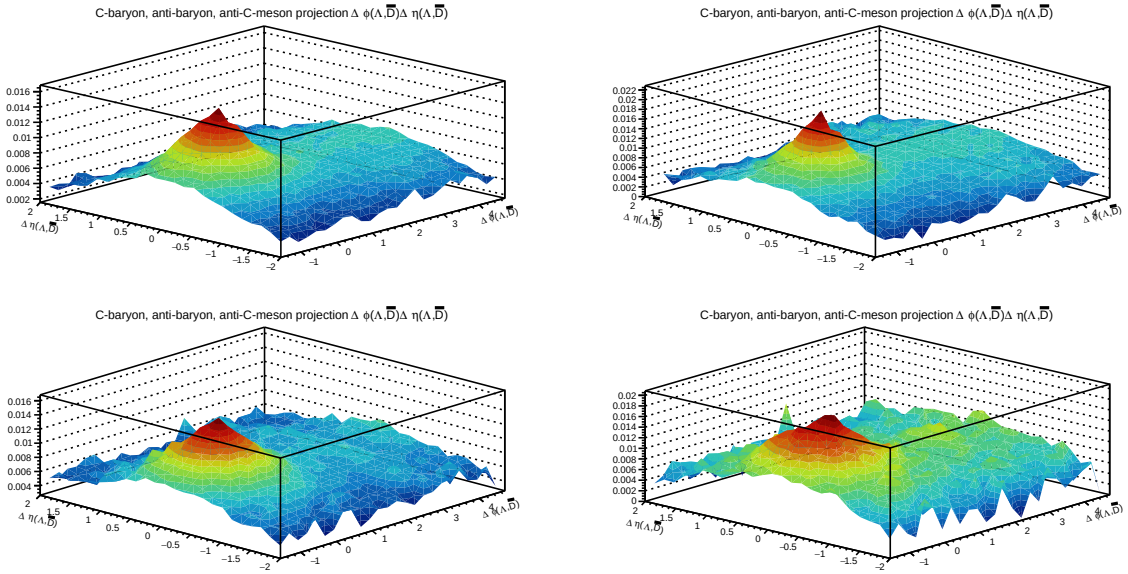

Figure 31: Opposite baryon opposite charm with applied ranges.

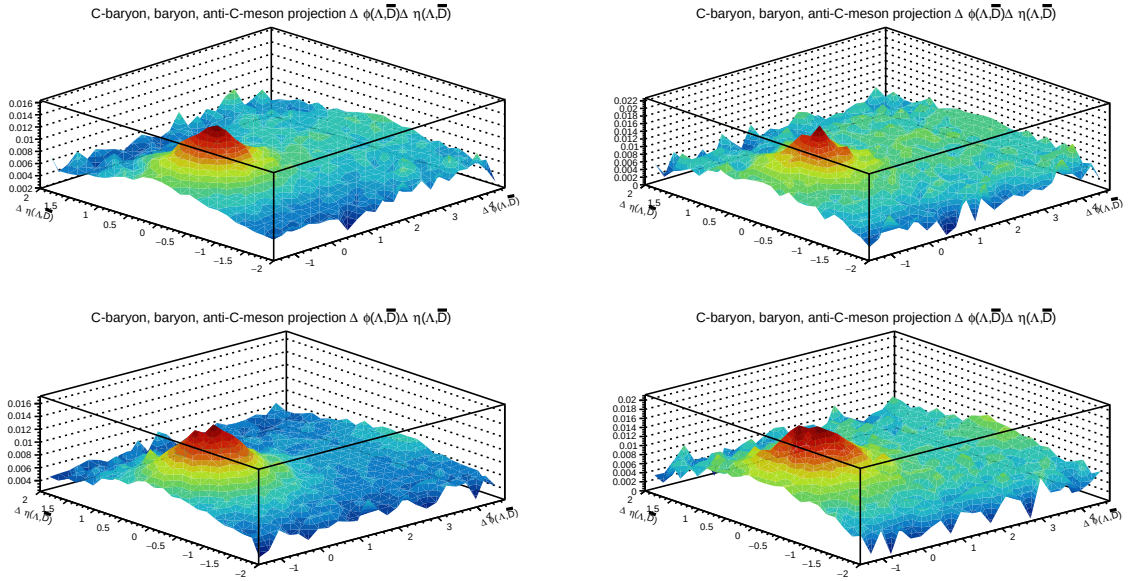

Figure 32: Same baryon opposite charm with applied ranges.

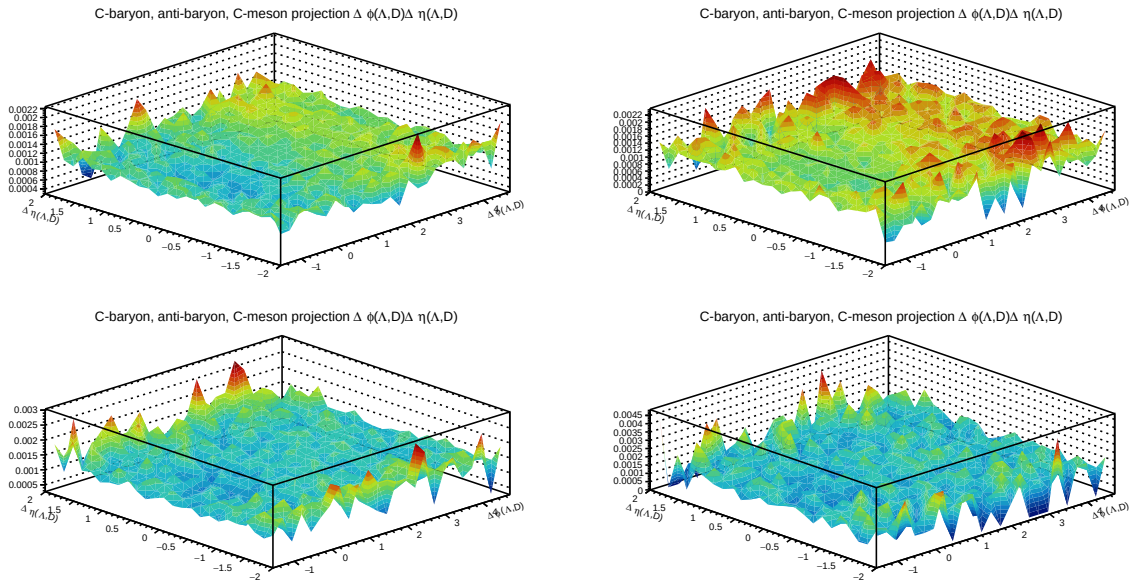

Figure 33: Opposite baryon same charm with applied ranges.

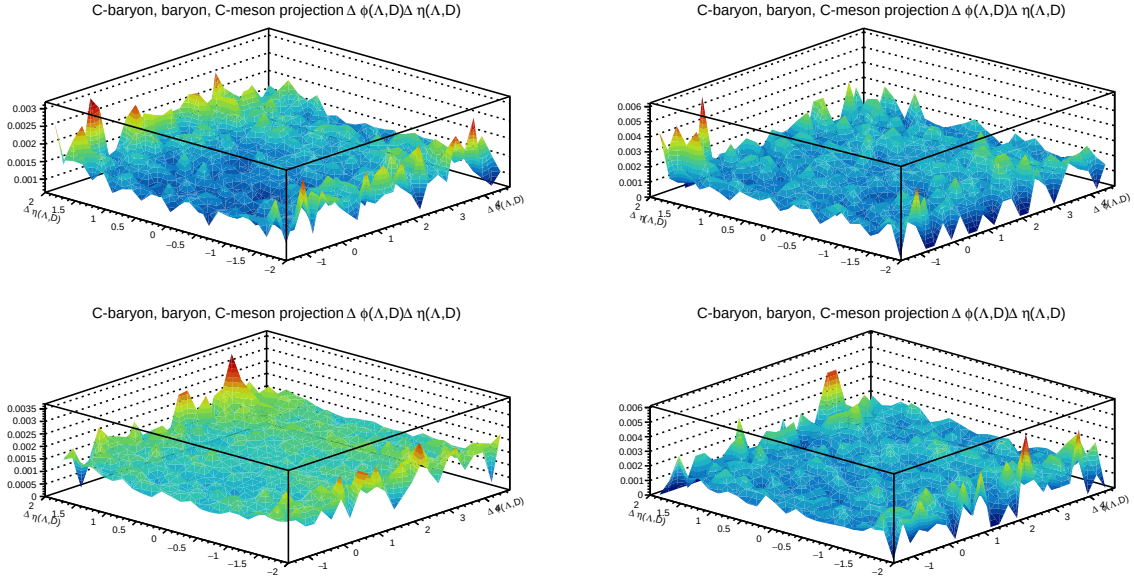

Figure 34: Same baryon same charm with applied ranges.

7.2.3 Ranges After Division

Below, the projections on $\Delta\phi_{\Lambda,D(\overline{D})}$ are shown for the fraction of the correlation function with set range over the correlation function without set range. The order is the same as in 7.1.2.

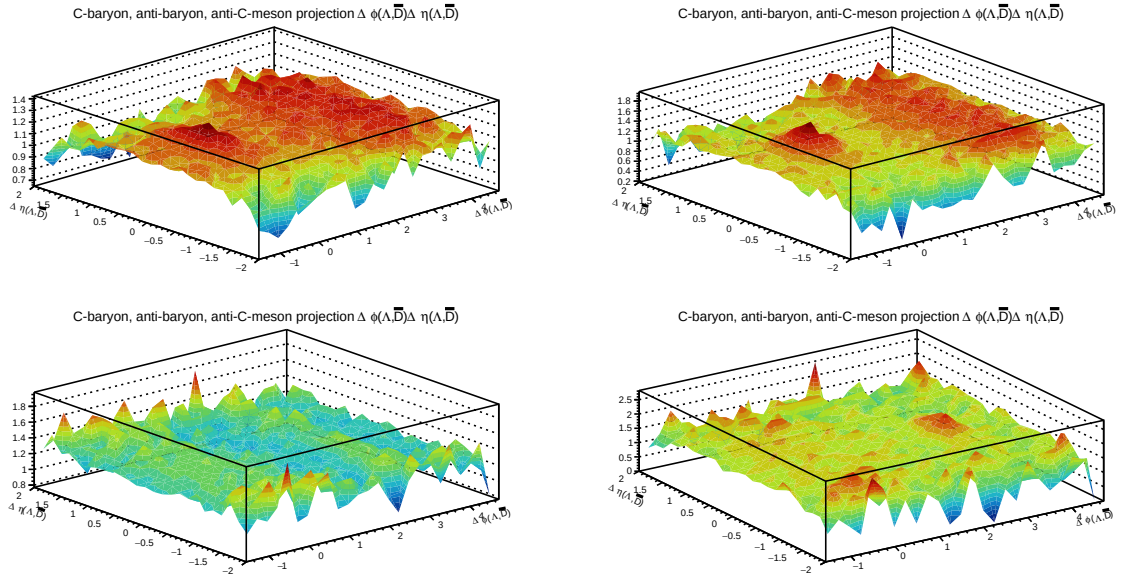

Figure 35: Fraction of range and no set range, opposite baryon opposite charm.

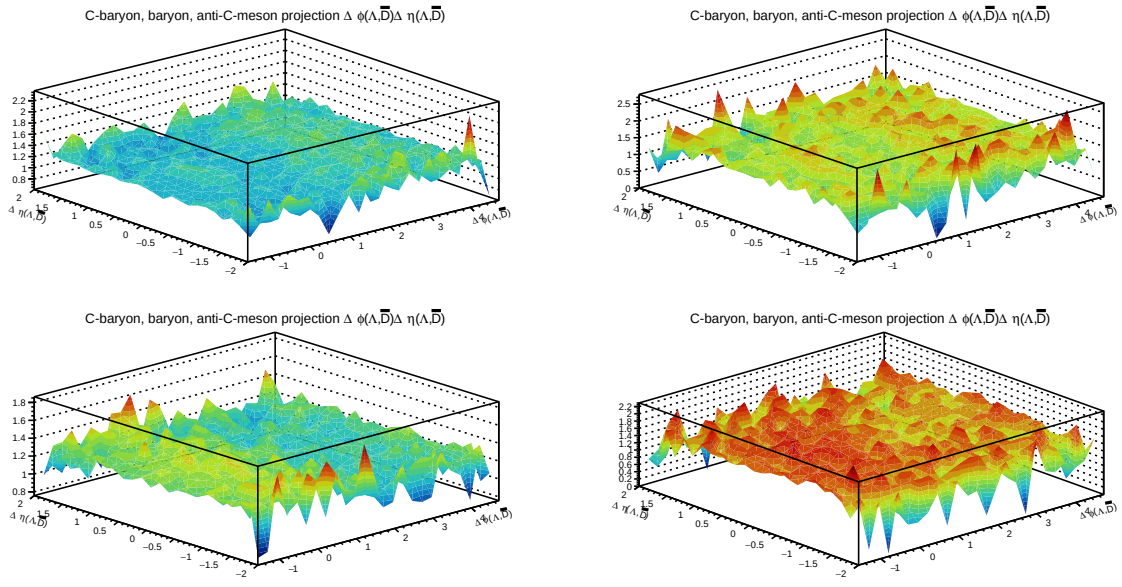

Figure 36: Fraction of range and no set range, same baryon opposite charm.

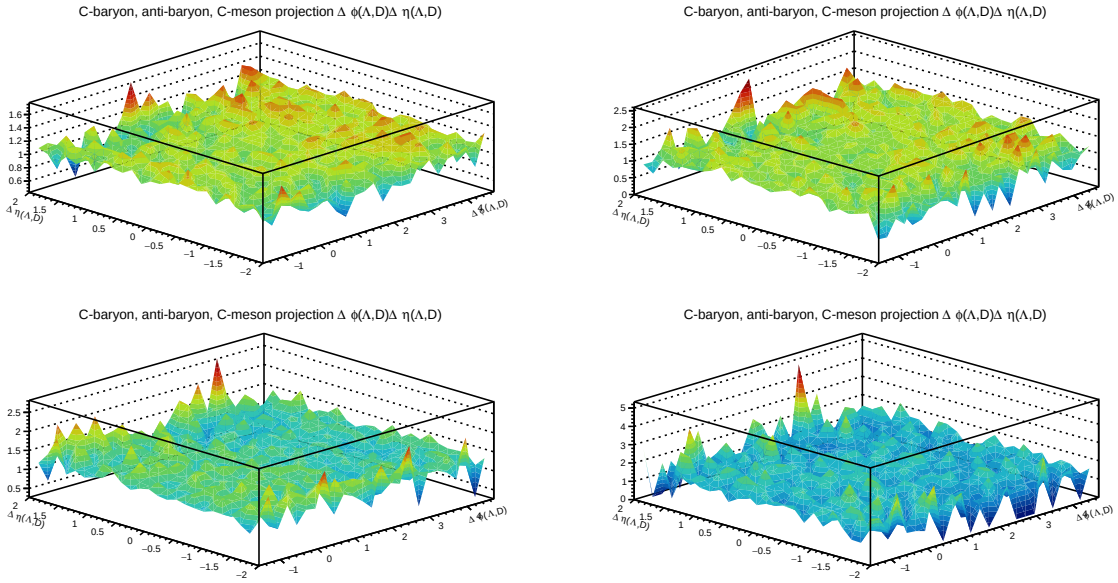

Figure 37: Fraction of the range and no set range, opposite baryon same charm.

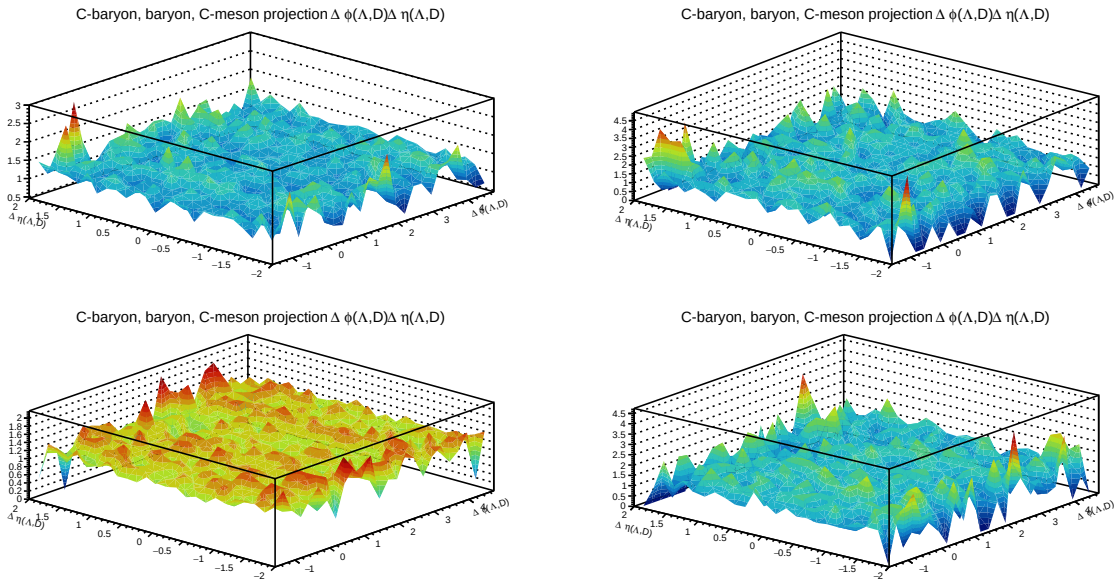

Figure 38: Fraction of the range and no set range, same baryon same charm.